NEW CONCEPTS FOR THE MOBILIZATION OF THE COMPONENTS OF SHEAR RESISTANCE IN CLAY

Review of a Large Experimental Study to Determine the Behavior of Mohr-Coulomb Cohesion and Friction in Clay

by John H. Schmertmann[1]

Prologue

The Managing Director of the NGI, Dr. Suzanne Lacasse, asked me to write a prologue to the paper to help the reader understand its unusual history. I will briefly review it here. It involves a long association with the NGI.

It all began when I met the first Managing Director of the NGI, Dr. Laurits Bjerrum, in early 1956 after he gave a lecture to graduate students and faculty at Northwestern University. I spoke with him afterwards and he kindly agreed to sell state-of-the-art, Geonor triaxial equipment to the University of Florida, where I started the university teaching and research part of my career later in 1956. By 1958 I had an operating laboratory and started my clay research for a PhD from Northwestern University with Dr. Jorj O. Osterberg as my advisor.

The ASCE's Research Conference on Shear Strength of Cohesive Soils at Boulder, CO in June 1960 gave me the opportunity to publish, together with Dr. Osterberg, the 1st major paper describing the research. By then the lab's Geonor equipment had expanded to that shown in the attached 1960 photo and we had developed and performed our first 100 **IDS**-tests.

Our paper attracted the attention of Dr. Karl Terzaghi, who made favorable comments about it in his taped introductory remarks to the Conference. Dr. Bjerrum, very active at this Conference, asked me to meet with him and Dr. A. Bishop in his hotel suite to discuss my research, at the end of which he invited me to come to the NGI for a year as a visiting post doctoral fellow. After completing my PhD at Northwestern in 1962 I moved my family to Oslo for 15 months, where I interacted with Dr. Bjerrum and the NGI staff and worked on various research projects and this clay research.

The NGI's invitation to participate in honoring Dr. Bjerrum after his sudden death in 1973 led to my 2nd major paper on clay shear in their 1976 Bjerrum Memorial Volume. It provides a summary of the 1958-1971 research and my thoughts about what we had learned. Then a 1978-2005 career change into consulting pre-empted any further major work to interpret the research results.

[1] Professor Emeritus, Dept of Civil and Coastal Engineering, University of Florida, Gainesville, FL 32611, email: schmert@ufl.edu. Please send discussions to the NGI at ngi@ngi.no with a copy to the author.

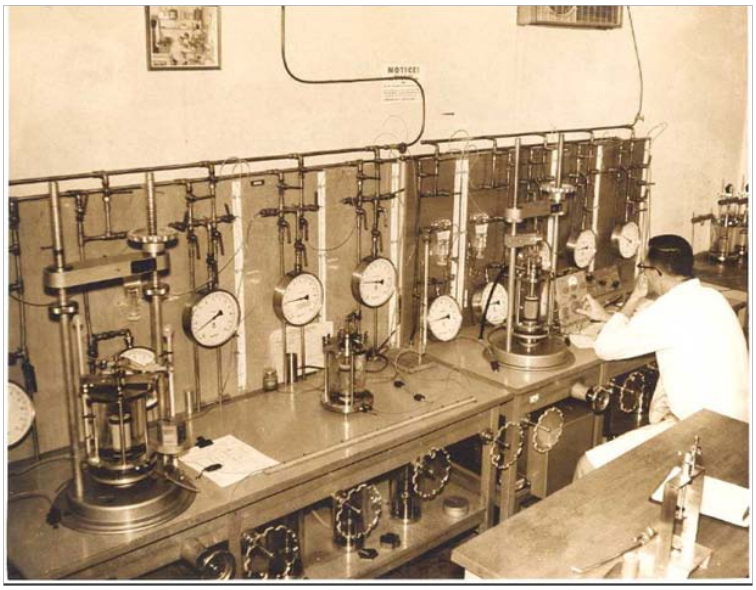

University of Florida Laboratory in 1960

NORWEGIAN GEOTECHNICAL INSTITUTE

ADDRESS: FORSKNINGSVN. 1, OSLO 3 - NORWAY — TELEPHONE 68 58 80

CABLE ADDRESS: GEOTEKNIKK, OSLO

Professor John H. Schmertmann
Department of Civil Engineering
University of Florida
Gainesville
Florida 32601
USA

Oslo, 16 November, 1966.
LB/et

Dear John:

I spent yesterday night reviewing once again some of the work you have been doing and looked in detail into the technique developed for studying the fundamental behaviour of our soils.

I would like you to know that I am more and more impressed by your work on this subject and I am pretty sure that your contribution is one of the most promising advancements in soil testing.

However, I am not writing this letter in order to give you my compliments. It is my hope that I can stimulate you to continue the work. I am feeling pretty strongly that you are able to with your technique to get much more results out of your testing. Most likely it requires a very much refined testing technique using much smaller jumps and measuring pore pressures electronically at the base of the sample, just as well as measuring the load inside the triaxial chamber. It is my hope that I can convince you to look into the details of what your testing technique in terms of results obtained during the early stage of a shear test. You might have to expand the type of material tested to include purely elastic materials such as rubber or rock samples, as well as purely frictional materials like steel balls. The paper you wrote on Hvorslev's parameters clearly showed me that you are next to putting your hands on something of a very fundamental type which we are all looking for, but have been unable to measure.

With my best personal regards,

Yours sincerely,

Laurits Bjerrum

Laurits Bjerrum's letter in 1966

Inspired by rediscovering Bjerrum's 1966 letter in 2005, I decided to make a complete review of my records from the research. This paper, the 3rd major work on the subject and an updated extension of the 2nd in the Memorial Volume, presents a "breakthrough" in my understanding. The reader will see how this evolved from an unsuspected, even paradoxical, special viscous friction behavior of the adsorbed water layer (AWL) on clay particles. This now seems obvious to me, but it did not appear so in the 1970's. Even Bjerrum missed it in his 1973 SOA paper. After making this mental leap all sorts of personal mysteries about clay shear behavior seemed to fall like dominoes and became at least partially resolved in my mind. The paper leads the reader through this personal experience of discovery and resolution.

It took a long time to happen, but this paper has now found a suitable "home" in one of the final printed volumes of a long and distinguished series of NGI publications.

ABSTRACT

This paper reviews a unique "**IDS**" triaxial test designed to separate the Mohr-Coulomb engineering components of shear resistance in soils. Selected results from approximately 500 such tests performed from 1958 to 1971 using saturated cohesive soils, from machine remolded to undisturbed, demonstrate important concepts, some new, about clay shear strength component behavior. These include: (1) The importance of considering strain and its effect on soil structure when measuring the components of shear resistance in clay. (2) A newly recognized "secondary" sliding **friction**, Φ'_{α}, that mobilizes fully at compressive strains of approximately 1% or less and likely results from the shear resistance behavior of an apparent viscous adsorbed water layer (AWL) between particle surfaces. (3) A "primary" friction, Φ'_{β}, measured directly by the **IDS-**test, that results from particle interference effects that mobilize more gradually with strain in laboratory normally consolidated (NC) clays. Overconsolidation (OC) and/or prior creep increase the subsequent strain rate of Φ'_{β} mobilization. (4) A viscous time transfer of AWL Φ'_{α} friction to the more stable Φ'_{β} friction. (5) A plastic cohesion, also likely due to AWL behavior, that provides a tensile strength even in machine remolded clays. (6) The formation of more permanent, but also more brittle, cohesive bonds during OC and/or ageing, and (7) A related practical discussion using the above concepts about the shear components to better understand residual friction, secondary consolidation and "secondary shear", ageing preconsolidation, silts, sands and partial saturation, undrained strength, the low-strain shear modulus, K_o, different types of consolidation, Burland's ICL, the minimum surcharge ratio for effective drainage aids, failure planes and slickensides, the shear components during creep, and similar components when testing drained or undrained.

Key words: adsorbed water layer, ageing, bonds, clay, cohesion, consolidation, creep, drained, drainage aids, double layer, effective stress, failure planes, friction, ICL, IDS-tests, K_o, preconsolidation, primary consolidation, primary shear, remolded, residual strength, secondary consolidation, secondary shear, shear, shear modulus, slickensides, time effects, tension, triaxial tests, undisturbed, unsaturated, viscosity.

TABLE OF CONTENTS

1. INTRODUCTION

In the early development of soil mechanics, say the 50 years from 1920-1970, many prominent researchers and engineers studied the shear strength of soils, particularly clays. For examples of some references over these 50 years that significantly influenced the research described in this paper see Bjerrum (1967a, 1972), Casagrande (1932), Horn and Deere (1962), Hvorslev (1961), Lambe (1953, 1958, 1960), Rowe and Rowe et. al. (1957, 1962, 1963, 1964), Skempton (1953, 1961, 1970), and Terzaghi (1920, 1931, 1941a, 1941b, 1955). However, many questions remain unanswered, such as the nature and importance of the adsorbed water layer (AWL) between clay particle contacts, the existence or non-existence of cohesion in unbonded clays, the reliability of cohesion, the origins of residual shear and secondary consolidation, and the reliability for practice when using ageing-preconsolidation in geologically NC clays. These and other questions still remain for many engineers. This paper provides another perspective and some possible answers.

Herein, as in all the previous reports of his shear resistance research, the writer used the Mohr-Coulomb (M-C) model to express the total shear resistance in cohesion and friction terminology. The following **simple definitions of "cohesion" and "friction"** apply in this paper. The writer assumed that the total mobilized shear resistance of a saturated soil structure subjected to shear loading consists of the sum of two sets of engineering components, as follows: The **cohesion components** that behave approximately independently of the magnitude of compressive effective stress and give a soil its tensile strength, and the **friction components** that depend approximately linearly on the magnitude of compressive effective stress and contribute no tensile strength. He also assumed that all mobilized components = 0 when the shear loading = 0.

The M-C model dominated early research, has the attraction of simplicity, remains in widespread use, and the research results summarized herein seem explainable using this model. But important alternatives exist. Critical State Soil Mechanics (CSSM), using Cam-clay and associated models as described by Schofield and Wroth (1968) and Schofield (1999, 2005), argue for the superiority of these newer models. But, to the writer's knowledge, none of these include a new soil "secondary" friction component with many unusual properties, cohesion in remolded clays, shear component changes with strain, and major time transfer effects between components. The laboratory test results presented herein do not at present fit easily into a mechanistic, continuum mechanics picture of clay shear resistance. But, as interpreted by the writer, they do fit in with the electrochemical, viscous behavior of the adsorbed water layer as described by Terzaghi (1920, 1931, 1941a, 1941b), Lambe (1953, 1958, 1960) and others.

The writer took an original approach to the experimental study of the shear strength of clays at the University of Florida from 1958 to 1971. During this time he and his students (the "we" herein) developed and performed approximately 500 axisymmetric triaxial tests of a then new type, referred to herein as **IDS**-tests and described subsequently, in a then state-of-the-art laboratory (See **14. ACKNOWLEDGEMENTS** and photo in the **PROLOGUE**). Publications authored or co-authored by the writer in 1960, 1962, 1963, 1964, 1976, 1981, 1991 and 1993, all referenced herein, document and summarize many of the previous findings from this research. Ho (1971 pp. 3-26) reviewed much of the M-C cohesion and friction component research and resulting theories over the years 1932-1971. This includes the **IDS-**test research, to which he added. This paper provides a fresh review of this research.

The catch-all word "structure" as used herein refers to a particular state of the extremely complex 'fabric' of the 3-dimensional packing and arrangement of particles and aggregates, its specific volume or void ratio, the attractive and repulsive forces and the resultant adsorbed water layer (AWL) on and between particles, and the cementation and other bonds that may form between particles or aggregates of particles. All soils have "structure". **Strain** distorts and changes structure. Schmertmann (1964) describes in some detail the need to consider strain and its effect on structure when measuring the components of shear resistance in clay.

The reader should treat all stresses as effective and, unless noted otherwise, all strains refer to axial compressive strains denoted by "Є" with the time-rate of strain denoted by "Ė". Some of the data and concepts presented herein may require more explanation than allowed by the length of this paper. The reader can supplement this paper by referring to the references cited and will find copies of many of these references in a website by using the following link: http://geotechnical.schmertmann.info/.

2. SUMMARY OF THE IDS-TEST

2.1 Preview of Shear Components

The writer's interpretation of the results from this large laboratory research program using the **IDS**-test led to the concepts developed herein. As a guide to this development, it might help the reader to see some of this interpretation in advance in the form of the summary Equation (5). Unfortunately, important strain and time effects such as strain rate and creep complicate any attempt to present a realistic yet simple equation to express the Mohr-Coulomb envelope shear behavior of clays. The writer offers the following equation (5) as a still simplified, but hopefully informative, summary of the components developed herein.

$$\{\tau = \mathbf{I}_c + \mathbf{I}_b + \sigma' \tan [\Phi'_\alpha + (\Phi'_\beta \approx \Phi'')]\}_{\epsilon,t} \quad \text{.....(5)}$$

Wherein:

- τ = Mobilized **shear resistance**.
- $\mathbf{I}_c$ = Plastic **cohesion**, probably slowly decreasing with reducing strain rate.
- $\mathbf{I}_b$ = Bond **cohesion**, generally relatively brittle and increasing with rest time at constant load.
- Φ'_α = Sliding **friction** through adsorbed water layer lubricant, viscous, decreasing with rest time, and also referred to subsequently as "secondary friction".
- Φ'_β = **Friction** due to particle/particle geometrical interference effects, increasing with OC, dry density, anisotropic consolidation, creep, secondary compression, and rest time, and clearly more stable than Φ'_α. Also referred to subsequently as "primary friction".
- ϵ,t = Subscripts denote that the mobilized shear and its components refer to the same axial strain at a particular time, and emphasizes they can vary with strain and time.

2.2 Explanation of the IDS-test

The writer developed the **IDS**-test as a **strain rate controlled**, **drained** triaxial test procedure for separating the apparent effective stress independent (**I**) and dependent (**D**) Mohr envelope components, 'nominal cohesion' and 'friction', respectively, as functions of initial structure and subsequent strain (**S**) – hence "**IDS**". Figure 1 shows the progress of an **IDS**-test in 4 steps, the first two experimental and the final two analytical.

Referring to Figure 1a, points A and B, unloaded from $\acute{\sigma}_c$, show the best locations in a consolidation load-unload cycle to have approximately (meaning 'close enough for the purposes of this research') the same after-consolidation structure, including void ratio, but with a measurable difference in effective stress. The researcher then subjects these two isotropically (in this research) consolidated specimens to triaxial compression, as in Figure 1b, and keeps each at a constant effective stress of σ'_{1A} and σ'_{1B}, respectively, by continually **controlling pore pressures** to match deviator stress while continuing the same axial strain rate. This produces a constant $\acute{\sigma}_1$, decreasing σ'_3 stress path.

Figure 1b* also shows schematically the stress-strain path of the test performed with a single specimen using the method described subsequently under **3.2 Curve Hopping**. At any strain, such as ϵ_X, specimen A will mobilize shear τ_{AX} and specimen B will mobilize a lower τ_{BX}, depending on the soil structure's reaction at ϵ_X to a change from σ'_{1A} to a lower σ'_{1B}. The researcher will then have measured directly a value of friction using two (or one) specimens with approximately the same initial structure

* In Figure 1b and generally herein, the writer refers to the **IDS**-tests as strain (Є) controlled with a constant rate of strain (Ė). But, more accurately, we performed them with a constant rate of downward movement of the top of a strain-gage load cell. We corrected for load cell and triaxial cell load column compressions. These compressions reduced Ė, especially during the low Є, high-modulus portion of a test. We also corrected for the vertical strains associated with the *c.* ½% volume strains during curve hopping.

EXPERIMENTAL STEPS

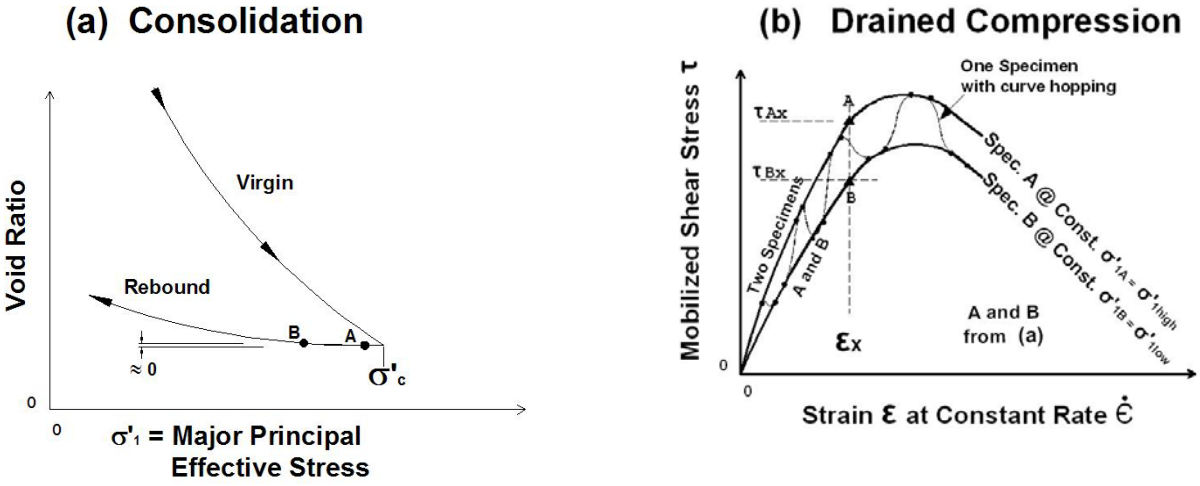

ANALYTICAL STEPS

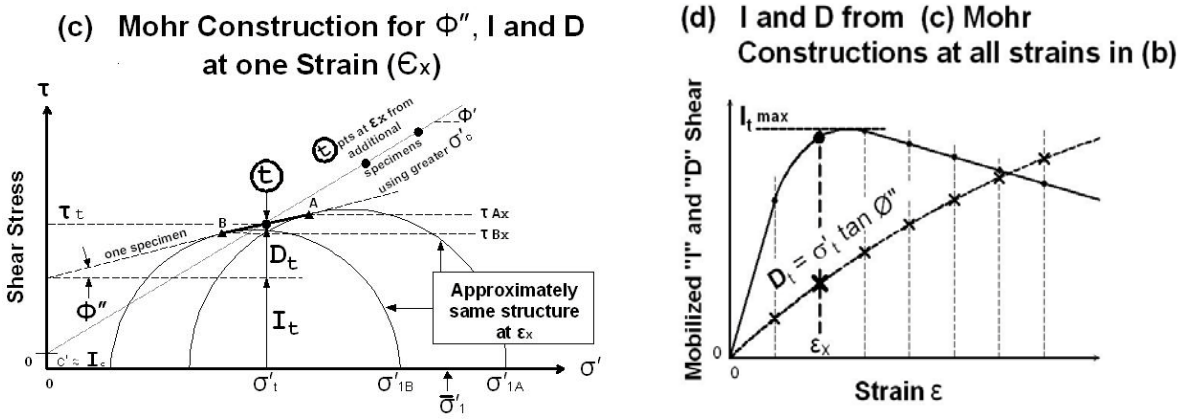

Figure 1: 4 Steps in Constant–σ´₁ IDS-test Using Either One or Two Specimens (Schematic)

along very similar stress and time paths to the same strain, and thus with approximately the same structure.

Figure 1c presents the Mohr circles representing the triaxial stress conditions at τ_{AX} and τ_{BX} as points A and B on the common tangent to the circles. The slope of this tangent gives an experimentally determined friction differential with a slope angle denoted Φ". The writer assumed this tangent slope correct at the midpoint "t" at effective stress σ'_t and shear stress τ_t. This assumption neglects a 1.5% too-low error in the **I** intercept resulting from envelope curvature between points A and B (Schmertmann, 1976 pp. 77, 78). Linearly extrapolating the A-B slope to the σ′ = 0 axis gives an apparent effective stress independent $\mathbf{I}_t$ component, or 'nominal cohesion', which leaves $\mathbf{D}_t$ as the directly measured, effective stress dependent friction component mobilized at σ'_t. The research by Schmertmann and Osterberg (1960, pp. 7-20), and a review by Schmertmann (1976, pp. 76-78), support this use of a linear extrapolation to obtain $\mathbf{I}_t$. Note from Figure 1c that:

$[\tau = \mathbf{I} + \mathbf{D}]_t$ ..... (1a)

$\mathbf{D}_t = \sigma'_t \tan \Phi''$ ..... (1b)

and that the writer often uses the angle Φ" or tan Φ" , and later also Φ'_β, to represent the **D** component.

The point "t" comes from one (any) strain in a single **IDS**-test. Finally, as shown in Figure 1d, one plots the $\mathbf{I}_t$ and $\mathbf{D}_t$ values for ϵ_X. Plotting the results from many strains from the same 1- or 2-specimen test in Figure 1b, using the method in Figure 1c, and connecting the points in Figure 1d produces the test objective of determining the mobilization of **I** and **D** with **S**train. **I** typically has a maximum value $\mathbf{I}_m$ at $\epsilon \leq 1\%$, shown schematically in Figure 1d.

3. TEST METHODS

3.1 Extruded Clays, Standard Procedure

Of necessity to have enough comparative test results, we used machine mixed and extruded (severely remolded) specimens. We extruded batches of approximately 40 clay specimens using a "Vac-aire" machine, described in Matlock et. al. (1951), wherein powered augers mixed the clay and forced it, in a vacuum to obtain near-saturation, several times through a 1,000 mm^2 circular die. We then cut the clay into 100 mm length specimen blanks, wrapped them in wax paper coated with a petrowax and stored them in a humid room. Some post-extrusion restructuring occurred. We used the blanks after storage of at least one month and only after determining by miniature vane shear tests that each batch's undrained strength had reached an approximate constant with time. Upon removal for testing, we trimmed each blank to an 80 mm test specimen length in a split miter box for mounting in a triaxial cell. The test specimens had a length/diameter ratio of 2.2, which we assumed high enough to avoid the complication of using frictionless platens. Altogether, we extruded and stored approximately 1,000 specimen blanks from a variety of clays. They had a typical degree of saturation of 99% and a preconsolidation $p_c \approx 50$ kPa from the extrusion and restructuring. Table 1 gives some classification information for these clays, which the writer chose based on availability, variety, availability of undisturbed specimens for comparison testing, and a high enough permeability for convenient **IDS**-test research. Air conditioning kept the temperature of the lab approximately constant within a range of 22° to 26°C.

To simplify comparisons between tests, and recognizing the importance of drainage rate and other time effects (discussed subsequently), we used the following approximate 'standard' procedure for most of the tests: (1) One day, one increment isotropic consolidation to σ'_c; (2) $\dot{\epsilon}$ control $\approx$ 1.0 %/t_{100} or less, where t_{100} = isotropic, primary consolidation time for $\approx$ 100% effective stress increase; (3) Drained test with pore pressure control for $\sigma'_1 \approx$ constant; and (4) Triaxial compression with constant $\sigma'_{1high} \approx 0.95\ \sigma'_c$ and $\sigma'_{1low} \approx 0.75\ \sigma'_c$. The resulting stress path kept σ'_1 below σ'_c to avoid abrupt yielding changes in the structure of the test specimen. Schmertmann (1962) includes an extensive discussion of the method, the accuracy requirements for the successful performance of such an **IDS**-test, and the experimental errors involved.

The volume change occurring during the above 20% σ'_c change in σ'_1 produced a typical 1/2 % volume strain. The writer also investigated a 10% to 60% change in σ'_1 and thus smaller and larger volume strains. As a result he assumed a 20% change produced a change in structure of negligible importance when separating the shear components (see Schmertmann and Osterberg (1960, pp. 649-662) and Schmertmann (1976, pp. 76-78)). The results in these references and herein support this assumption.

Usually only the variable under study would differ from the 'standard procedure'. Using machine extruded clays also had the important advantage of mechanically destroying most or all of any cohesive bonds that had formed in the natural clay due to cementation or other insitu ageing effects. Test results from extruded clays provided a good destructured baseline from which to measure differences

Table 1: Plasticity and Mineralogy of Clays Tested (from Schmertmann 1976)

Extruded Clay	Plasticity Index (PI %)	-0.002 mm. %	Activity PI/-0.002	Clay Minerals
Enid (residual)	9	20	0.45	Kaolinite – 15% Illite – 10%
Jacksonville	14	13	1.08	Montmorillonite – 10%
Boston blue kv $\approx 6 \times 10^{-9}$cm/s	19	53	0.36	Illite – 45% Chlorite – 25%
Kaolinite kv $\approx 3 \times 10^{-8}$cm/s	21	60	0.35	Kaolinite – 99%
Lake Wauburg	105	85	1.24	Montmorillonite – 85% Illite – 5%

when comparing with the same clay when testing a restructured or an undisturbed specimen.

3.2 Curve Hopping

Schmertmann and Osterberg (1960, Figs. 1-13) describe the learning transition from performing **IDS** (then called "CFS")–tests using up to five duplicate specimens versus the two shown in Figure 1, and eventually to only a single specimen using a "curve hopping" technique (Figure 1b). This technique involves imposing controlled and continuous pore pressure changes on the specimen during its continuing drained compression and hopping back and forth between the two levels of σ'_1 and determining successive points along each σ'_1 hop. Connecting final "●" points before the next hop forms 'dash' increments along each σ'_1 curve. Then one connects the 'dashes' to estimate the two complete curves as if the hopping had not occurred. Schmertmann (1962) showed 15 comparisons between 1 and 2 specimen **IDS**-tests from a variety of extruded and undisturbed soils. They confirm the practical validity of the use of a single specimen with the curve hopping, **even with 'undisturbed' specimens**.

3.3 Uniform Pore Pressure

An accurate drained, strain-controlled **IDS-**test requires that the controlled pore pressures applied at the specimen base distribute practically uniformly throughout. The writer believes we attained this goal by using a combination of drainage and monitoring techniques, including: 1) External filter strips and caps, 2) One or more needle-punched 1.8 mm diameter longitudinal **internal** drains filled with saturated, twisted wool yarn, 3) Occasional check tests using slower rates of strain to allow more time for pore pressure uniformity, and/or using back pressure to force 100% saturation, and/or checking uniformity with pore pressure needles, 4) Using strain rates based on the prior measured time for isotropic consolidation and thus link rate to the actual specimen drainage, permeability and stiffness conditions, and 5) Monitoring the progress of the above described curve hopping and using only the final two data points when they both appeared to have reached the next σ'_1 level curve, as in Figure 1b. See Schmertmann and Osterberg (1960, pp. 648-668) for a description of the development of test procedures designed, in part, to assure uniform pore pressure.

4. MOHR ENVELOPE RESULTS FROM EXTRUDED CLAYS

The conventional c′-Φ′ Mohr envelope usually presents the results of strength tests as the linear or curved tangent to a sequence of Mohr circles at different stresses and void ratios, each at some given shear strength condition such as maximum shear. The condition could occur at different strains. Thus, the circles and envelope could apply to different structures with a different mobilization of the components of shear resistance. Again, see Schmertmann (1964, 1976 pp. 65-66).

Herein the writer uses a variation–with the envelope defined by the locus of tangent points ("t" in Figure 1c) from a sequence (see below) of **IDS**-tests at the **same strain**. This permits introducing test strains, and their effects on clay structure and shear mobilization, into the study of the components of clay shear. The reader will soon see that such Mohr envelopes using a constant strain have little or no curvature when testing 99% saturated, nominally normally consolidated (OCR = 1.05 and 1.33 during the **IDS-**test for σ'_1 = 0.95 σ'_c and 0.75 σ'_c, respectively) extruded clays within the 50 to 700 kPa range of σ'_c investigated. The OCRs given subsequently refer to values before the **IDS-**test.

The following envelopes in Figures 2, 3 and 5 come from comparing **IDS**-test results from many nearly duplicate extruded specimens, each test providing a point "t" as shown in Figure 1c, with each envelope for a different constant axial strain Є. Most of the data points in the subsequent figures result from tests that substantially followed the 'standard procedure' but had different magnitudes of isotropic consolidation σ'_c, and therefore of void ratio, σ'_{1h}, σ'_{1l}, and σ'_t.

4.1 Normally Consolidated (NC) Clays

Note that Figures 2a and 3a show data and shear component envelopes for the total ($\mathbf{I}_t + \mathbf{D}_t$) components, = τ_t, versus σ'_t, and Figures 2b, 3b and 5 only show data and envelopes for the $\mathbf{I}_t$ component versus σ'_t.

Figure 2a shows comparative τ_t versus σ'_t results from extruded Boston blue clay (BBC) at representative compressive strains of ϵ = 0.5, 4.0, and 10.0%. A computer has fit a least-squares straight line through the individual test data points with each point weighted equally. The numbers next to each line indicate the slope angle (Φ'), the extrapolated zero intercept (c') and the R^2 value of the linear fit, which in this figure varies from 0.949 to 0.999. All the subsequent R^2 values also fall within this range and support the validity of the linearity of the Mohr envelopes over the stresses, strains and strain rates investigated.

Figure 2b shows the results from the same tests but with only the $\mathbf{I}_t$ component instead of the total $\tau_t = \mathbf{I}_t + \mathbf{D}_t$ mobilized shear in Figure 2a. The numbers denote the slope angle (Φ'_α), the extrapolated zero intercept ($\mathbf{I}_c$), and R^2. Note the dramatic difference versus Figure 2a – all three strains plot almost identically. $\mathbf{I}_c$ and Φ'_α do not vary much with strain and in this respect appear to behave plastically over the axial strain range of 0.5-10%.

Figures 3a and 3b show the similar results obtained from a commercial kaolinite powder mixed with distilled water (reconstituted). Comparing the extruded kaolinite with the Boston blue clay provides one example of how reconstituted kaolinite matches test results in natural clays. Kaolinite, used extensively in this research, has many desirable properties for laboratory research. See Schmertmann (1963) for more information about the kaolinite used and the usefulness of kaolinite.

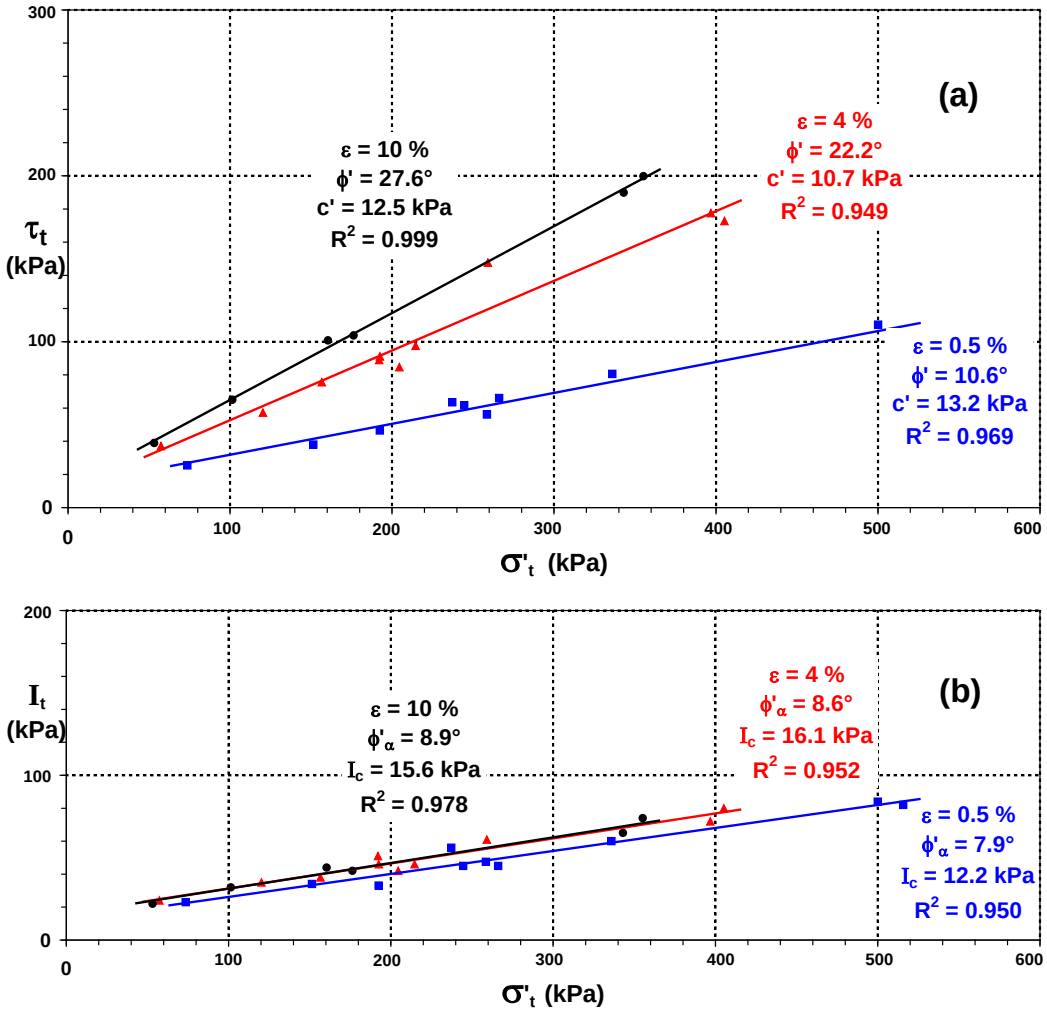

Figure 2: IDS-test Mohr Envelopes, Extruded NC Boston Blue Clay

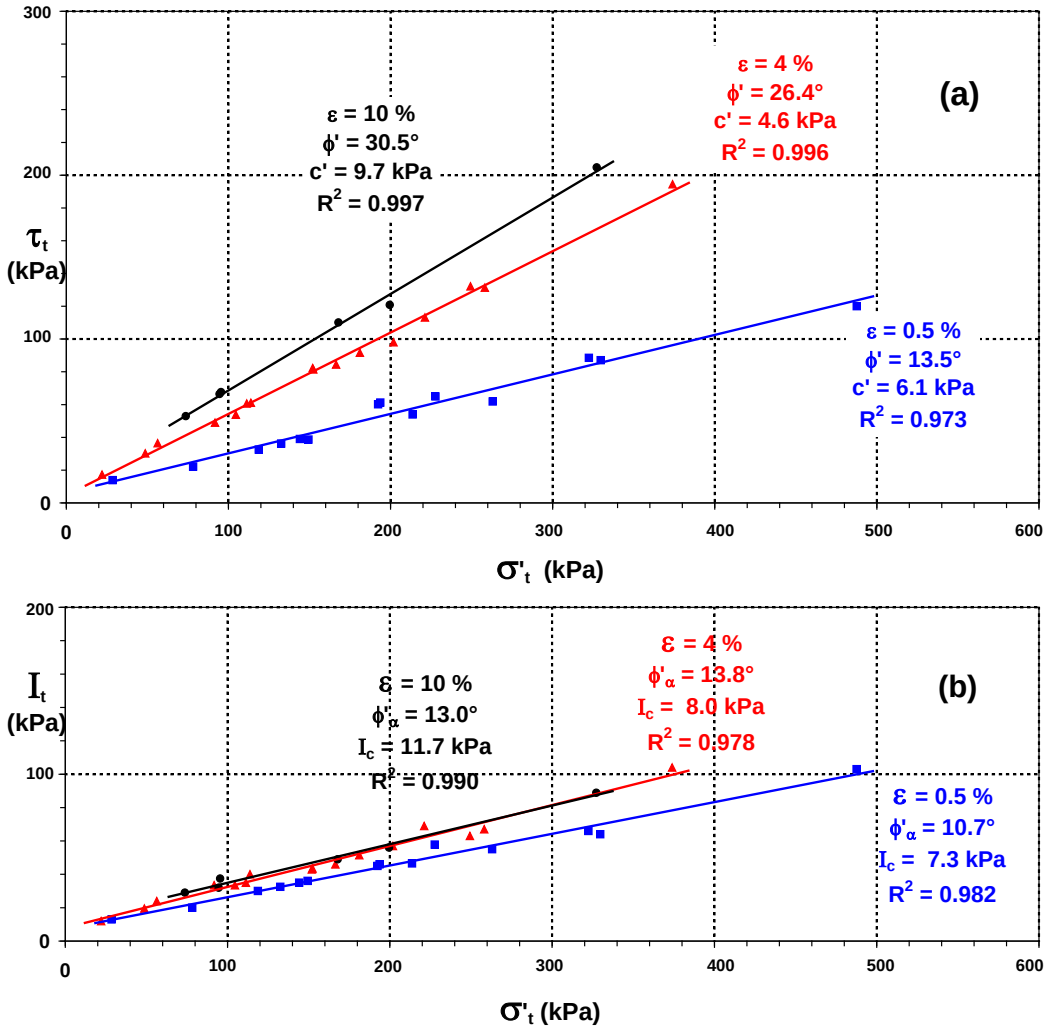

Figure 3: IDS-test Mohr Envelopes, NC Kaolinite

4.2 Normally Consolidated (NC) versus Overconsolidated (OC) Clays

4.2.1 Kaolinite Clay

Figure 4, based on Schmertmann (1976, Figure 6), presents results from a sequence of isotropic NC and OC consolidation tests followed by **IDS**-tests. As discussed below, they demonstrate further the remarkable insensitivity of the **I** component to clay structure, for example its void ratio, dilatancy and OCR, and also its linear dependence on effective stress over the stress range investigated. Figures 2b and 3b have already shown this linearity.

Figure 4a shows an arithmetic void ratio versus major principal effective stress σ'_1 graph of the results from four normally consolidated specimens (test Nos. 111, 112, 106, 105) and five overconsolidated specimens (test Nos. 107, 109, 110, 108, 113). All the test specimens came from the same batch of extruded clay with the narrow range of computed initial void ratios shown. The figure shows the position on the graph of each specimen after NC or OC and the variation of σ'_1 and void ratio during the **IDS**-test curve hopping at the axial strain of the maximum value of **I** = $\mathbf{I}_m$, which typically occurred at Є≈1%. Figure 4c shows the key to reading the void ratio and σ'_1 changes associated with consolidation, rebound, and the **IDS**-test curve hopping at the strain of $\mathbf{I}_m$.

Figure 4b shows the values of $\mathbf{I}_m$ (see Figure 1d) from each test using the same effective stress scale as in Figure 4a, with each point located at the average $\overline{\sigma}'_1$ of the test σ'_{1h} and σ'_{1l} values. Clearly, void ratio does not significantly affect $\mathbf{I}_m$ – compare the three test groups 111-113, 112-108, and 106-107-109-110, each group with decreasing void ratios but at approximately the same effective stress.

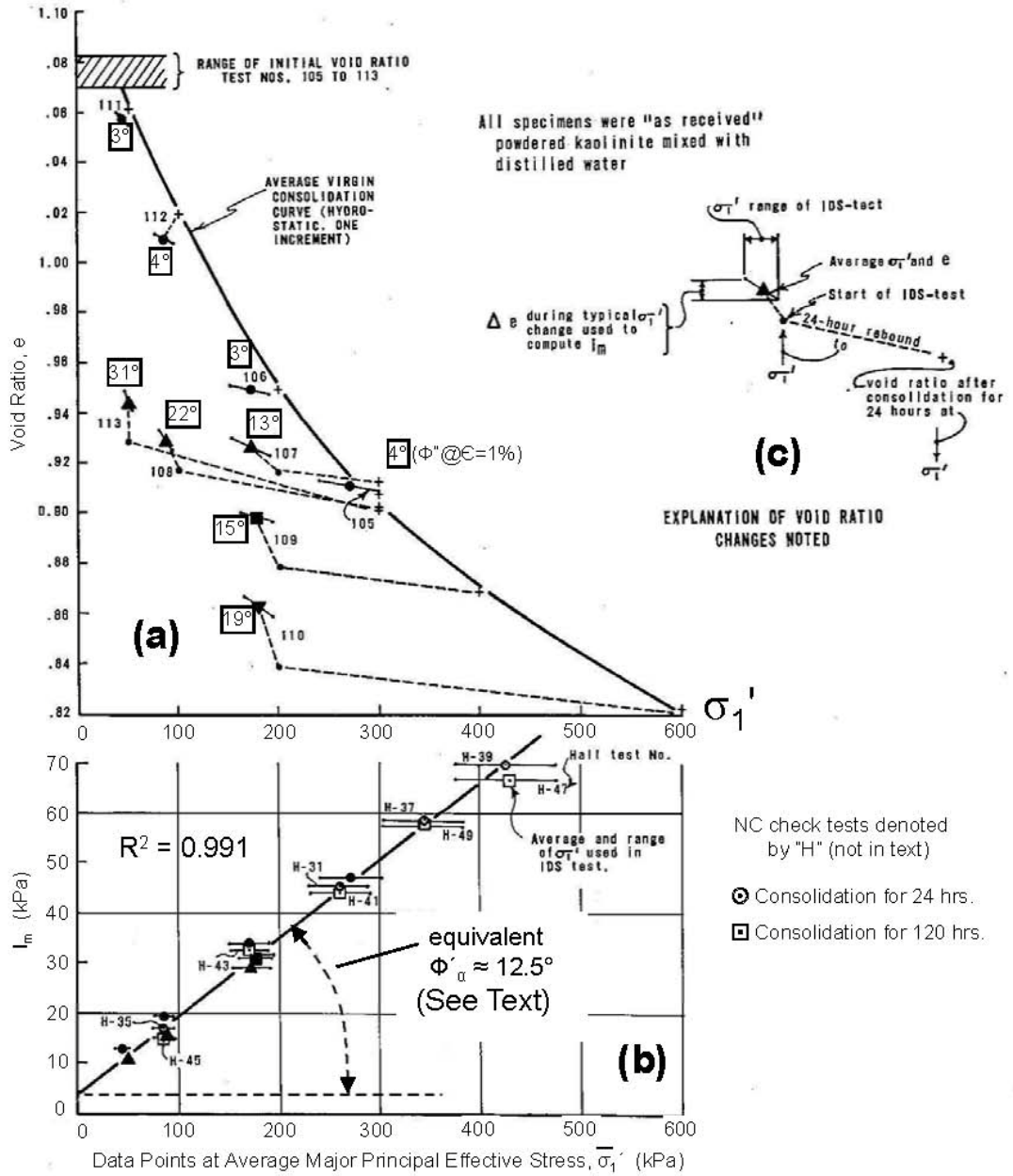

Figure 4: Demonstration of I_m independence from void ratio, dilatancy, secondary consolidation time and OCR in extruded kaolinite (annotated from Schmertmann 1976)

Unlike the approximately constant $\mathbf{I}_m$, Φ″ increases with the progressive reduction in void ratio due to the increase in the OCR within each of these three groups – with Φ″ increasing from 3° to 31°, 4° to 22°, and 3° to 19°, respectively.

However, $\mathbf{I}_m$ does vary with effective stress – consider test group (105-107-108-113) at roughly the same void ratio but with an approximate five-fold reduction in effective stress and $\mathbf{I}_m$. Figure 4b shows convincingly that $\mathbf{I}_m$ in kaolinite depends linearly on $\overline{\sigma}_1'$ and not on void ratio.

The **IDS**-test results in Figure 4 also show something important concerning $\mathbf{I}_m$ and dilatancy, interlocking and friction. The NC-OC test pairs 111-113 and 112-108 had contractant and dilatant structures (- and + dilatancy), respectively, yet each pair had ≈ $\mathbf{I}_m$. The sequence of tests at the same effective stress but with progressively increasing +dilatancy, test Nos. 106, 107, 109, and 110, also have ≈ $\mathbf{I}_m$ despite the OCR increasing from 1 to 3.

Our experience with kaolinite showed that $\sigma'_t \approx 0.70\ \overline{\sigma}_1'$. Figure 1c shows why $\sigma'_t < \overline{\sigma}_1'$. The writer converted $\overline{\sigma}_1'$ to the equivalent σ'_t

to get the equivalent Φ'_α angle in Figure 4b. This $\Phi'_\alpha \approx 12.5°$ at the $\mathbf{I}_m$ strain ≈ 1% and fits nicely within the Figure 3b values of $\Phi'_\alpha = 8.0°$, 13.8° and 13.0° at strains of 0.5, 4 and 10%, respectively. If dilatancy results primarily from particle interlocking effects, the above data show that dilatancy and interlocking have only a minor, if any, effect on $\mathbf{I}_m$ and Φ'_α in extruded kaolinite over the strain interval of at least 0.5-10%.

The writer will show subsequently that Φ'_α represents an unexpected component of clay friction. If true, we have the unusual situation of a friction not sensitive to OC and interlocking. This requires an unusual explanation, also given subsequently.

4.2.2 Enid Clay

Note that the writer also performed an unpublished series of tests similar to those in Figure 4 using the extruded natural residual Enid clay, with similar results, and obtained $\Phi'_\alpha \approx 13.2°$ from this series.

Figure 5 shows an $\mathbf{I}_t$ versus σ'_t graph from **IDS**-tests using Enid clay, similar to those shown in Figures 2b and 3b except it shows only the data points and linear fit for a representative $\epsilon = 4\%$. In addition it shows results from three **IDS**-tests on specimens with overconsolidation ratios of OCR = 2, 4 and 7. They fit almost exactly on the best fit line for the NC tests. This provides another example, in addition to that shown for the kaolinite in Figure 4, that the **I**-component depends on effective stress but not on the OCR.

As expected, these OCR tests in Figure 5 produced a clearly stronger OC versus NC Mohr envelope (not shown). Figure 4 just showed that $\mathbf{I}_m$ at a given $\overline{\sigma}'_1$ remains approximately constant at all OCRs investigated. Any increase in mobilized shear in Figure 5 at $\epsilon = 4\%$ must result from an increase in $\mathbf{D}_t$, or Φ''. Figure 5 shows the measured increases in $\Phi'' = 6.1°$, 11.9°, and 18.7° for OCR = 2, 4 and 7, respectively, when compared to Φ'' at $\epsilon = 4\%$ when only NC to the reduced σ'_{cu} that produced the OC. These increases in Φ'' explain the stronger OC versus NC envelope.

5. APPARENT PARADOX

Figures 2b, 3b, 4b and 5, from tests on extruded NC and OC clays, all show the **I** component linearly dependent on effective stress with an extrapolated $\sigma'_t = 0$ intercept. Schmertmann (1976, Figure 11) provides further evidence of this linearity from other clays, a silt and two sands. This reference provides still further evidence from **undrained IDS**-tests on three **undisturbed**, soft clays in Figures 17, 18, and 19 as explained therein. Ho (1971 p. 79) also confirmed this linearity in great detail using specimens of extruded kaolinite and glass spheres. The writer therefore considers it well established that this linear relationship exists, to the maximum σ'_c = 700 kPa investigated, in some, and probably many, remolded and undisturbed clays, silts and sands.

The above leads to an apparent paradox, expressed as follows:

> *The ($\mathbf{I}_t$ - $\mathbf{I}_c$) component obtained from the Figure 1c linear extrapolation to the effective stress origin as part of a nominal cohesion intercept presumed independent of effective stress, instead increases linearly with applied effective stress.*

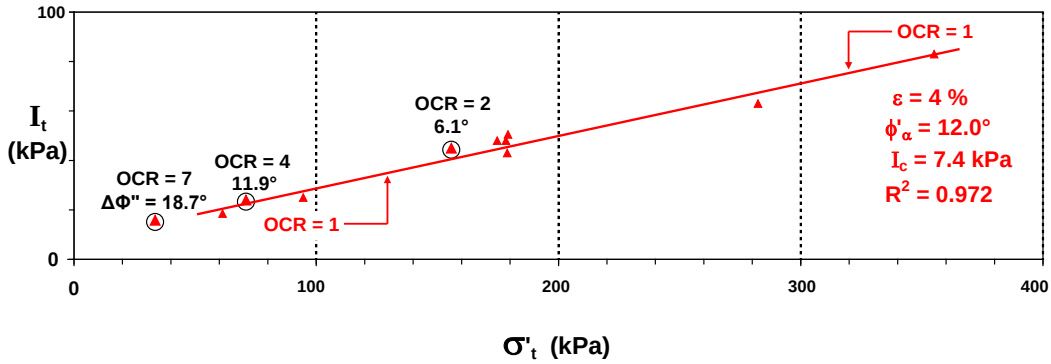

Figure 5: IDS-test Mohr It Envelope, Extruded NC and OC ENID Clay at $\epsilon = 4\%$

Therefore, whatever the detailed reasons for such linear behavior, ($\mathbf{I_t}$-$\mathbf{I_c}$) **behaves as an engineering friction** with an angle here denoted Φ'_α and a value denoted $\mathbf{I}_\alpha$. Equation (2) expresses this friction:

$$\mathbf{I}_\alpha = (\mathbf{I_t}\text{-}\mathbf{I_c}) = \sigma'_t (\tan \Phi'_\alpha) \quad \text{.....(2)}$$

The writer's subsequent explanation of this apparent paradox involves the viscous friction behavior of the adsorbed water layers (AWLs) on clay particles and seems consistent with other data about Φ'_α behavior and with Terzaghi's (1941a and 1941b) concepts. He called it "liquid friction" in 1941b. **The demonstration herein of a viscous Φ'_α friction, whatever the detailed reasons for the apparent viscous and friction behavior, should and does help explain the unique engineering behavior of clay.**

6. COHESION IN EXTRUDED KAOLINITE

The kaolinite's $\sigma'_t = 0$ intercepts of c′ and $\mathbf{I}_c$ at $\dot{\epsilon} = 0.5$, 4 and 10% in Figure 3 suggest that a real cohesion may exist at the 'standard' $\dot{\epsilon} \approx 0.007$%/min. The c′ intercepts in Figure 3a = 6.1, 4.6, and 9.7, and average 6.8 kPa. In Figure 3b the $\mathbf{I}_c$ intercepts = 7.3, 8.0, and 11.7, with an average of 9.0 kPa. As part of our comprehensive effort to prove or disprove that the extruded kaolinite had a real cohesion, one of the writer's students, Topshøj (1970), also performed 8 NC and 6 OC, constant σ'_1, kaolinite **IDS extension** tests. They produced a similar $\mathbf{I}_c$ = 8.4 kPa using $\mathbf{I}_m$ at an average ϵ = -2.5%. Now consider the results from two **non-IDS** test methods.

Topshøj (1970) also checked directly the mobilized shear with zero effective stress on the plane of shear by performing a series of 11 Bishop and Garga (1969) type effective stress triaxial tension tests on hourglass-shaped duplicate specimens of the same kaolinite used for Figures 3 and 4. Figure 6 shows the maximum-shear Mohr's circle from each test. The then difficult-to-measure-accurately tensile strains for each point varied from -0.4 to -2.4%, with an average of -1.14%. Topshøj used an axial strain rate that she deliberately varied between $\dot{\epsilon} = 0.0015$ to 0.015%/min, and concluded that this rate variation had no significant effect on the $\mathbf{I}_o$ result in Figure 6. Note the greatly expanded scale to show the detail at low stresses, and that 8 of the 11 circles extend into effective tension at maximum shear. All tests had an imposed zero pore pressure at specimen mid height via a base drain connection to an external tank with a free water surface.

All the specimens apparently failed in shear, some with a visible network of parallel shear planes. The writer determined an approximate failure plane angle of 29° from horizontal from her tests. The points on the Mohr circles in Figure 6 show the mobilized shear on that average plane. A least squares linear fit through the points gives a σ′= 0 shear mobilization intercept of $\mathbf{I}_o$ = 7.7 kPa. The scatter in the data points results from the experimental difficulties with accurately measuring small effective stresses, and initial differences between the extruded duplicate specimens, all emphasized by the expanded scale. Considering Topshøj had 11 tests, the writer believes she

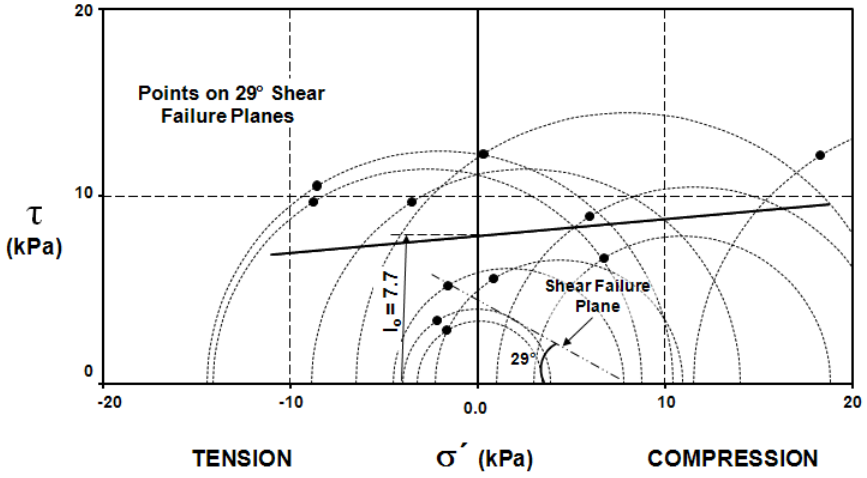

Figure 6: I_o from Tension Tests on Extruded Kaolinite

had sufficient data to support the $\mathbf{I}_o$ = 7.7 kPa cohesion intercept in this kaolinite when testing at $\dot{\epsilon}$ = 0.0015 to 0.015%/min.

The tension tests in Figure 6 all increased void ratio, or dilated, during the test. The work to dilate against cell pressure might account for some or all of the cohesion intercept. Topshøj (1970, pp. 65-68) corrected for the work involved using the method in Rowe (1962), which reduced $\mathbf{I}_o$ approximately 30% to 7.7 kPa. The writer believes that capillarity (computed avg. 99.9% saturation), negative pore pressures (slow strain rate), dilatancy (corrected), and experimental error (all known significant errors corrected) did not produce this 7.7 kPa cohesion from these tension tests. Topshøj (1970) also performed four NC, back-pressured, compression stress-dilatency tests using the Rowe et.al. (1963) method and obtained an average 8.3 kPa for the cohesion intercept, with ϵ from 0.3 to 1.9%. These 7.7 and 8.3 kPa results from non-**IDS** tests also fit within the aforementioned c´ and $\mathbf{I}_c$ of 6.8 and 9.0 kPa from the two **IDS-**test methods. The writer therefore believes that all these results from a comprehensive investigation prove that a real cohesion existed in this kaolinite clay. If it can exist in a reconstituted-from-powder, low activity, machine mixed and extruded saturated clay, it seems likely it can and does exist in most or all natural clays at the strain rates investigated. However, its magnitude may depend on strain rate. See **11.2 $\mathbf{I}_c$ Reliability** for further discussion of rate effects.

7. LINKING IDS AND CONVENTIONAL TESTS ($\Phi'' \approx \Phi'_\beta$)

Figure 7 shows the graphical link between Φ'' from an **IDS-**test and a new, subsequently explained, Φ'_β as determined from Φ in Figures 2a and 3a minus Φ'_α from Figures 2b and 3b. $\Phi'_\beta = (\Phi' - \Phi'_\alpha)$ at the same strain as Φ''. Equation (3) expresses the link mathematically.

$$\tan \Phi'' = \sin \Phi'_\beta / [\cos \Phi'_\alpha \cos (\Phi'_\alpha + \Phi'_\beta)] \quad \text{..... (3)}$$

Using typical values of Φ'_β and Φ'_α in equation (3) shows Φ'' exceeds Φ'_β, usually by less than 2°. For the purposes of this paper the writer considers this difference minor and assumes $(\Phi' - \Phi'_\alpha) = \Phi'_\beta \approx \Phi''$ and will use Φ'' and Φ'_β interchangeably.

8. THE MOHR ENVELOPE COMPONENTS OF EXTRUDED SHEAR RESISTANCE AND THEIR TIME DEPENDENCIES

Figure 8 shows a schematic diagram of the Mohr envelope components of mobilized shear resistance as demonstrated in this paper from the results of many **IDS** triaxial compression and some extension and tension tests (Topshøj, 1970), on extruded, isotropically consolidated, near-saturated, duplicate specimens. The data herein comes from only three extruded clays but the previously cited references refer to similar data from other clays,

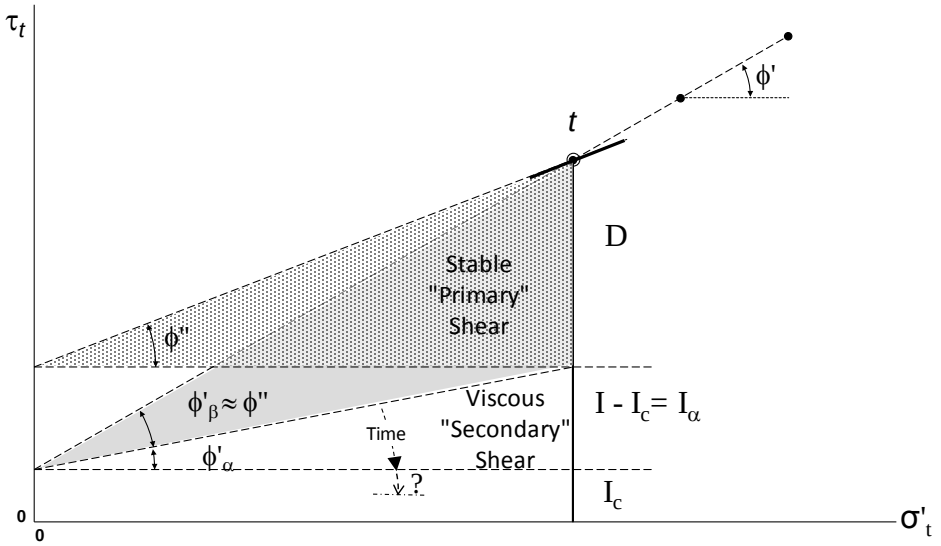

Figure 7: Test Ø˝ ≈ Ø´-Ø´$_\alpha$ = Ø´$_\beta$ "Secondary" and "Primary" Shear (Also see Figures 1c and 8, Equation 2)

including 'undisturbed', and also from silt, sands, and glass spheres.

Working from zero to increasing shear in Figure 8, we first have the cohesion component $\mathbf{I}_c \approx c'$, approximately constant with strain, which this paper demonstrates behaves as a real cohesion by showing a comparable tensile shear strength in one example clay. Section **10** discusses a possible additional, more brittle bond cohesion, $\mathbf{I}_b$. The next component, the $\sigma'_t \tan \Phi'_\alpha$ part of **I**, or $\mathbf{I}_\alpha$, has a range of approximately 8-14° in the extruded and 'undisturbed' clays investigated, and in compression usually has only a minor dependence on axial strain after **I** develops fully at $\epsilon \approx 1\%$.

The third and last component, herein denoted Φ'_β, which, as discussed in the previous section, approximately equals the Φ soil friction component demonstrated directly by the **IDS**-test. In NC clay it increases slowly and roughly linearly with strain, at least to strains of approximately 5%. Figure 8 illustrates a typical value of Φ'_β for a strain of 10%. Note that at ϵ=10% the clays tested had nearly reached their maximum **IDS**-test drained shear mobilization. Thus the 10% envelope in Figure 8 would also approximately match the c'-Φ' conventional maximum drained shear envelope. Figure 8 also shows schematically how the additional mobilized shear in overconsolidated clays at the same 10% strain produces a stronger envelope that results entirely from additional Φ'_β ($\approx \Phi''$). It appears, from previous and with subsequent further discussion under **9.3 Explanation of Φ'_β,** that Φ'_β results from particle geometrical interference effects.

Early in the **IDS**-test research, which began in 1958, it became obvious that the shear components of the clays tested exhibited significant time effects, especially during time with constant shear, including zero shear. The **D-**component increased with time, usually accompanied by a measurable decrease in the **I**-component. The following Sections **8.1** to **8.5** present some examples from a variety of test conditions to illustrate the generality of this time-transfer behavior and its importance. For additional details and related testing see the references cited.

8.1 Undrained Creep with Shear

Bea (1960, 1963) performed and discussed **undrained** compression creep tests and results from specimens of machine extruded kaolinite and extruded and undisturbed Boston Blue Clay (BBC). After 2½ to 19 days of undrained creep using stress control, he performed an **IDS**-test on each specimen to determine the change in shear components, at the same strain, after creep versus results from an **IDS**-test after undrained compression with strain control and no creep. For all three clays he found that creep produced an increase in the **D** (or Φ'' or Φ'_β) component and a decrease in the **I** component. A short extrapolation back to the strain at the end of creep showed that the **IDS**-tests mobilized a shear resistance at the same axial strain that increased from 10-13% due to the prior creep. The soil structures had stiffened and particle geometrical interference effects had increased during the time of creep. For example, the extruded kaolinite's Φ'_β after

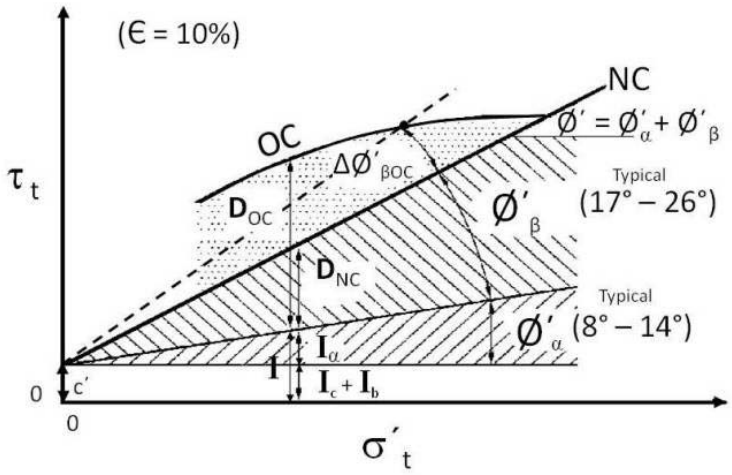

Figure 8: Schematic Summary of Components (NC, OC Extruded Clays)

19% strain had increased from 24° to 33° while **I** dropped from 27 kPa to near 0. The reader will also find details from Bea's tests in Schmertmann (1976, p. 87 and 1981, p. 472).

8.2 Drained Stress Control with Rest Time versus Strain Control

Strain control testing imposes a forced, continuing axial strain on a test specimen and allows little or no time for the structure to rest at constant shear load and develop any rest-related ageing effects. In contrast, stress control with increments of loading spaced after periods of constant-load rest does permit the soil structure time to adjust and develop rest-related ageing effects. Now consider the example in Figure 9a.

The strain-controlled test (solid lines) used the previously described curve hopping technique and used only a single specimen tested to a strain of 2.3% in 29 days with $\dot{\epsilon}$= 0.079%/d. The stress control test, tested over 37 days to a strain of 3.6%, used two duplicate specimens with 12 increments of loading and approximate three day rest periods between increments, for an average $\dot{\epsilon}$= 0.097%/d. We used one specimen for the same constant high σ'_{1h} used in the strain control test, and a duplicate specimen for the same constant low σ'_{1l}. Both stress control curves show the strain after each increment's 3 days of drained creep. They clearly show greater response to the same σ'_{1h} to σ'_{1l} change in effective stress, or in other words a greater Φ'' or Φ'_{β} versus the strain control test. We then followed each with an **IDS**-test component analysis (see Figure 1c,d).

Figure 9b shows the comparative **IDS**-test component results from stress versus strain control. The 1-specimen strain control test produced the usual rapid increase in **I** followed by constant or slowly decreasing **I** with additional strain (see Figure 1d). In contrast, the 2-specimen stress control test reaches the same initial maximum **I** but then **I** drops abruptly with further strain to 45% of its initial value at a strain of 2.3%. Over the same strains the Φ'_{β} (**D**) component increased substantially from approximately 11° to 18° at 2.3% strain. This figure provides an example of the time transfer of **I** to **D** when allowing versus not allowing periods of rest under constant load with similar average axial strain rates.

8.3 Rate of Strain ($\dot{\epsilon}$)

Although the rate of strain in a strain-control test does not have a major effect on the mobilization of the **I** and **D** components at a given strain and on the time transfer from **I** to **D**, it does have a measurable effect when considering orders-of-magnitude changes in strain rate. Part (a) of Figure 10 provides an example from extruded specimens of kaolinite at ϵ=1%. **I** decreased from approximately 60 to 50 kPa while Φ'_{β} increased from approximately 3 to 6° over a strain rate reduction factor of approximately 300. It appears that a sufficiently small strain rate and the increased time involved will permit some **I** to **D** transfer even with a con-

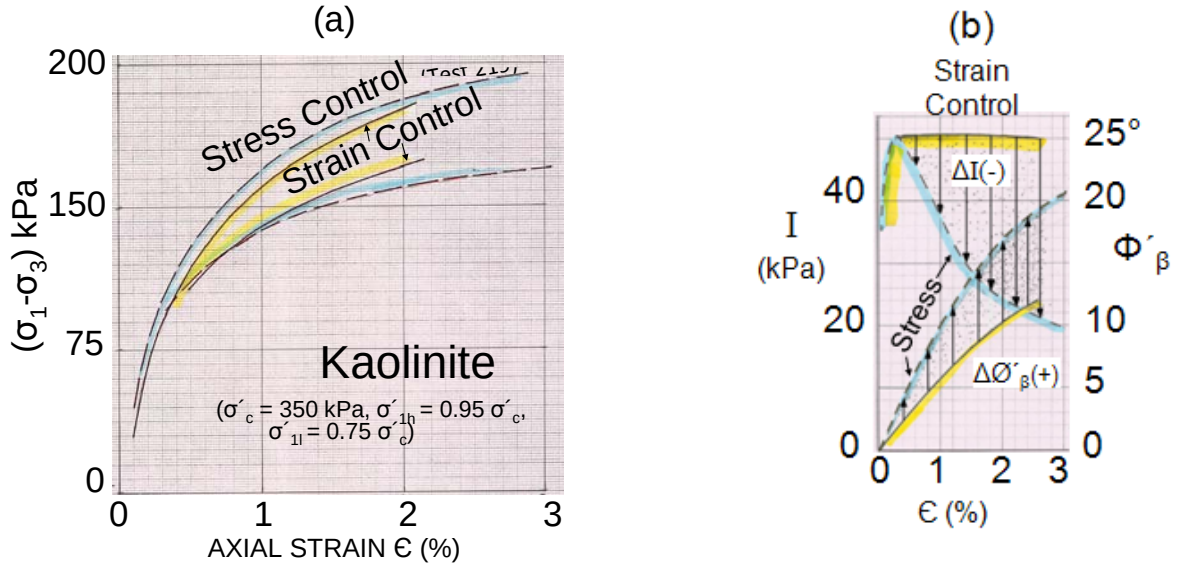

Figure 9: 29 Day Strain versus 37 Day Stress Control IDS-tests

tinuously forced strain increase. A subsequent discussion in **10.1** under **BOND COHESION** will consider part (b) of Figure 10.

8.4 Secondary Consolidation (Drained Creep without Applied Shear)

We also learned early in this research that longer times for isotropic secondary consolidation increased the mobilization of **D** in a subsequent **IDS-**test while leaving the **I** component somewhat reduced. For example, in one series of kaolinite tests increasing the secondary time from 100 to 52,000 minutes increased Φ'_{β} at Є = ½% from 1° to 6° with **I** decreasing from 52 to 45 kPa. In another series of four undrained tests the compression modulus over the (σ'_1-σ'_3) interval of 10 to 50 kPa increased from 900 to 8,800 kPa when the secondary time increased from 115 to 35,600 minutes. These and other comparisons provided clear evidence of significant soil structural changes resulting from secondary consolidation. The changes

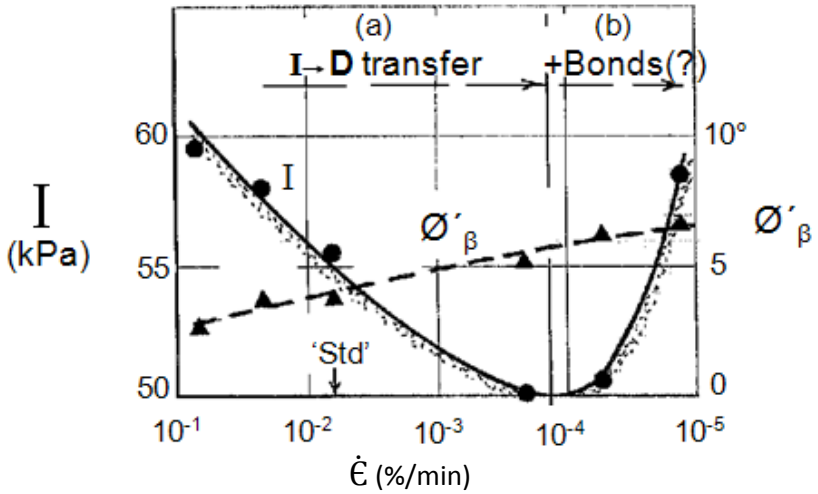

Figure 10: Effect of IDS-test Strain Rate on Kaolinite Shear Components @ ε = 1%

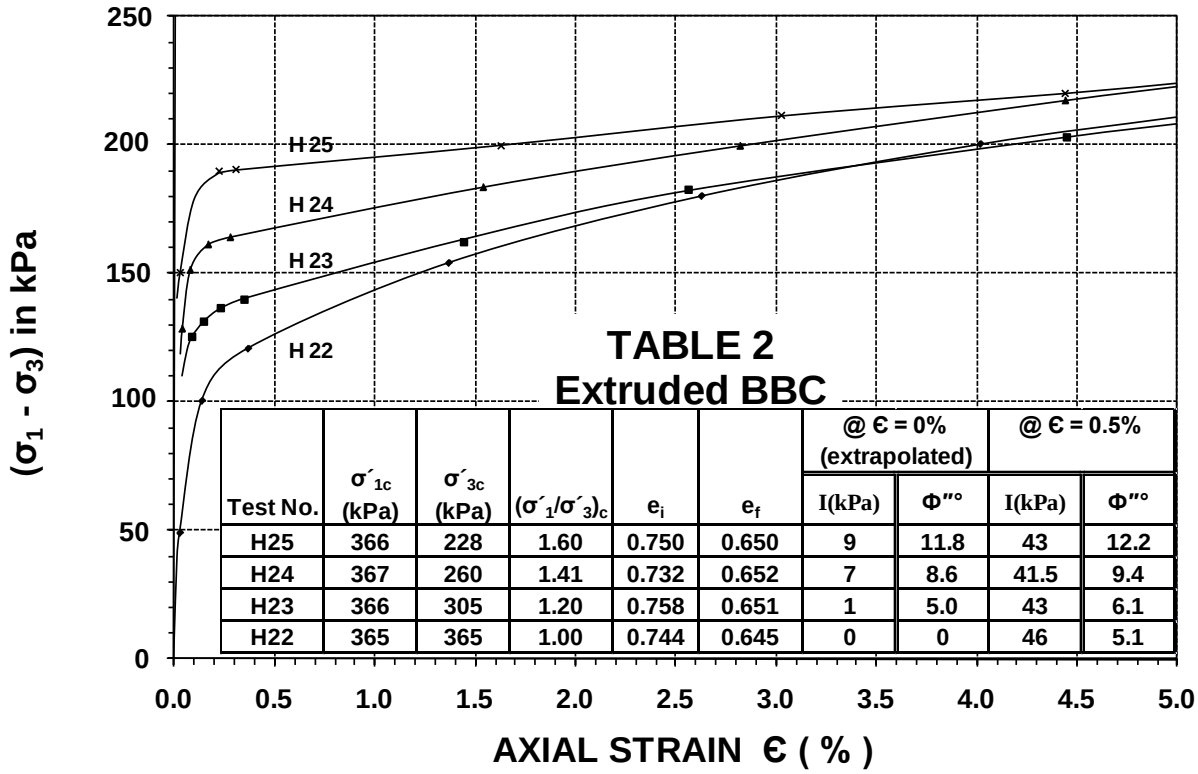

TABLE 2
Extruded BBC

Test No.	σ'_{1c} (kPa)	σ'_{3c} (kPa)	$(\sigma'_1/\sigma'_3)_c$	e_i	e_f	@ Є = 0% (extrapolated) I(kPa)	@ Є = 0% (extrapolated) Φ"°	@ Є = 0.5% I(kPa)	@ Є = 0.5% Φ"°
H25	366	228	1.60	0.750	0.650	9	11.8	43	12.2
H24	367	260	1.41	0.732	0.652	7	8.6	41.5	9.4
H23	366	305	1.20	0.758	0.651	1	5.0	43	6.1
H22	365	365	1.00	0.744	0.645	0	0	46	5.1

Figure 11: Superposed IDS-test axial stress curves at constant σ'_{1h} = 343 kPa versus Strain, after Anisotropic, Normal Consolidation, with related details in Table 2.

produce an increase in Φ'_β. The reader can find other and more detailed information about secondary consolidation and **IDS** component effects in Schmertmann (1976, p. 87; 1981 p. 474; and 1991, Figs. 27-30).

8.5 Anisotropic Consolidation (Drained Creep with Shear)

Schmertmann and Hall (1961) devoted an entire paper to showing the **IDS**-test shear component results after the 24h and 120h anisotropic, normal consolidation of extruded kaolinite and Boston blue clay over the $(\sigma'_1/\sigma'_3)_c$ range of 1 to 1.6. In all cases the **D**-component increased to carry the additional shear as this ratio increased. At the same time the **I**-component decreased. We thus found an **I** to **D** (or Φ'_α to Φ'_β) transfer during drained creep with shear. Also see Schmertmann (1976, Figure 23).

To illustrate the above consider the data in Figure 11. The figure shows comparative **IDS**-test σ'_{1h} curves from one series of extruded, duplicate BBC specimens after various levels of 24h anisotropic NC. As with the aforementioned secondary consolidation, the increase in the **D**-component (or Φ'_β) produces stiffening and strengthening of the clay's structure over a limited additional strain of about 4% in this case. Table 2 in Figure 11 gives the components and other comparative information when this additional (to consolidation) strain = 0 (using a short back-extrapolation) and at 0.5%. The reader can see how **D** (or Φ''_β) increased gradually and **I** dropped to near-zero at $\epsilon = 0$ and then increased abruptly, to typical isotropic consolidation values, at $\epsilon = 0.5\%$ as the anisotropic consolidation ratio increased from 1 to 1.6. At a ratio of 1.6, which is $1/K_o$, the mobilized compressive strength increased 50 percent at 0.5% additional axial strain due to the **I** to **D** time transfer induced by the anisotropic consolidation. This occurred despite the NC octahedral $(\sigma'_1 + 2\sigma'_3)/3$ effective stress at $\epsilon = 0.5\%$ decreasing from 2.59 kPa in H22 to 2.14 kPa in H25 and their almost identical void ratios.

9. ADSORBED WATER LAYER (AWL)

The possible importance of the adsorbed water layer (AWL) on the surface of all wet soil particles, but especially clays, has provided a subject of interest and controversy since the early years of soil mechanics. As shown below, this paper now continues by presenting more examples supporting its importance in the shear and consolidation behavior of clays.

Bjerrum (1973 p. 126) showed that undrained shear strength data requires a correction for rate of shear effects. Leroueil (1996), showed that viscous shear effects in clays produced a 27% increase in the preconsolidation stress p_c in the more rapid CRS versus CLI oedometer tests. He also showed a 40% increase in p_c when strain rate increased by a factor of over 1000 and how decreasing temperature also increased p_c due to its effect of increasing shear viscosity. Perkins and Sjursen (2009) showed that a *c.* 20°C decrease from lab room to N. Sea seabed temperatures increased Troll clay s_u and p_c by *c.* 20%, using "very good" to "excellent" quality undisturbed samples. Similarly, the profession has known for a long time that increasing temperature in the laboratory versus insitu also increases the rate of secondary consolidation. Anderson and Richart (1974) provide an example, also discussed in Section **12.6**. What might cause these significant effects in the shear resistance of clays? The writer believes that the special and viscous behavior of the adsorbed water layer surrounding the typical layer-lattice clay mineral particles provides the most likely answer.

Horn and Deere (1962, Table 1) showed a dramatic difference between the saturated and dry sliding friction (each denoted tan Φ'_μ in the subsequent Table 3a) shear behavior of "massive-structured soil minerals" such as quartz, feldspar and calcite, versus the "layer-lattice minerals" (now called phyllosilicates) common in clays. The massive minerals **increase** their sliding friction coefficient with saturation and the layer-lattice minerals **decrease** theirs. The decrease factor for the clay minerals in Table 3a averages 2.2. The authors referred to water as an "antilubricant" for the massive minerals, and as a "lubricant" in the layer-lattice minerals. Many lubricants behave as thin low-friction

layers, which leads to the writer's explanation of the Section **5** paradoxical Φ'_{α}.

Table 3: Comparing Clay Mineral Φ'_{μ} with Saturated Clay Φ'_{α}

(a) Minerals

Clay Minerals[1]	**tan Φ'_{μ}**	
	dry	**saturated**
Biotite	0.310	0.130
Chlorite	.529	.220
Muscovite	.431	.231
Phlogopite	.310	.149
	Avg = 0.395	**Avg = 0.183**

[1] From Horn and Deere (1962), Mitchell (1993)

(b) Clays

Extruded Clays (in this paper)	**tan Φ'_{α}**	
	dry	**saturated**
Kaolinite (avg. of 3), Fig. 3	0.543[1]	0.222
BBC (avg. of 3), Fig. 2		.148
Enid, Fig. 5		.212
		Avg = 0.194

[1] From one not-extruded test (Schmertmann, 1976, Fig. 10)

9.1 Explanation of Φ'_{α}

The left side of Figure 12 shows Terzaghi's (1941a, 1941b) concept of the interaction of the adsorbed water layers in contact around two solid soil particles. The relative thickness of the layer to the particle size, the shear and normal forces acting across the contacts, and time, determine the closeness of the particles to each other. Time implies a viscosity that increases with closeness due to colloidal effects. This, in turn, determines the hydraulic properties of the water between the particles, including its ability to transmit pore pressures. Particles with the AWL effectively squeezed out have an effective solid particle-particle contact with associated more rigid bonding, a very high AWL viscosity, and little or no pore pressure transmission over the contact area. That part of the water between particles relatively far apart has little viscosity and can transmit full pore pressures. In-between distances have 'contacts' with in-between viscosities and pore pressure transmission capabilities.

On the right side of Figure 12 the writer has greatly simplified the contact between two particles and their AWLs as transmitting full pore pressure over the area (A – a) and no pore pressure over the area "a" of a contact, with "A" representing the total shear section area per contact. Recognizing that the ratio (a/A) probably has a very small value, the math suggests that the sliding shear resistance through the contacts represents the tan Φ'_{α} frictional part of the **I**-component. This assumes a negligible contribution from Φ'' in the extruded clays, because at low strain Φ'' mobilizes much slower with strain than Φ'_{α} (compare **D** or Φ'' with **I** versus ϵ in the schematic Figure 1d and in Table 2). The subsequent Figures 17 and 18 suggest that Φ'', or Φ'_{β}, will mobilize even slower in natural clays because any bonding therein will inhibit the early strain development of Φ'_{β}.

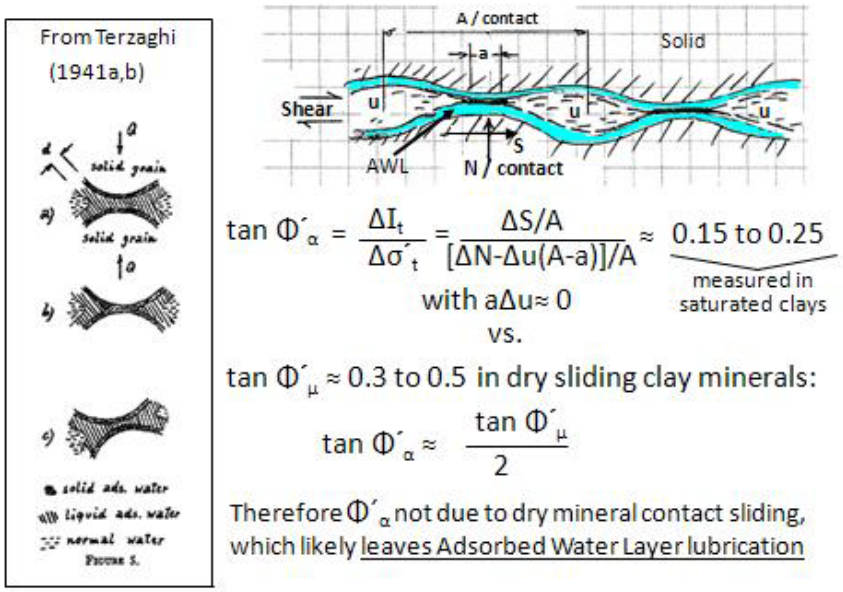

Figure 12: Paradox likely due to lubrication by adsorbed water layer

Now consider in Table 3 how the extruded clay (tan Φ'_α) values developed herein compare with the sliding friction (tan Φ'_μ) values along cleavage planes in some layer-lattice (phyllosilicate) minerals typical in clays. In such minerals water reduces Φ'_μ as detailed in Horn and Deere (1962) and summarized by Mitchell (1993) and in Table 3a. The writer added the previously documented saturated clay (tan Φ'_α) values into Table 3b. The (tan Φ'_μ) values range from 0.130 to 0.231, with an average of 0.183. The (tan Φ'_α) values range from 0.148 to 0.222, with an average of 0.194. A coincidence? Possibly, but the writer does not think so. These and subsequent data show that the paradoxical AWL Φ'_α from **IDS**-tests ≈ the sliding Φ'_μ in saturated clay minerals.

9.2 Φ'_α varies with d_{10}

If the shear behavior of the adsorbed water layer determines Φ'_α, and colloidal theory indicates the relative importance of this layer increases with a reduction in particle size, then it seems reasonable to expect a relationship between Φ'_α and particle size. Figure 13 shows a graph of Φ'_α versus d_{10} (log scale) from ten 'soils', including the three extruded BBC, kaolinite and Enid clays. The other seven soils include three clays-one from **undrained IDS**-tests using undisturbed specimens of a Norwegian, soft, Manglerud quick clay from Schmertmann (1976, Fig. 17) and identified by "U", a finely ground quartz silt, two sands, and glass spheres. The writer then added a $\Phi'_{residual}$ point from a mixed sandy, clayey silt from under the Pisa tower (see **12.1**).

Figure 13 suggests a roughly linear, semi-log relationship between Φ'_α and d_{10}. This provides further evidence, in the form of Φ'_α, for the existence and importance of the adsorbed water layer in clays, with reducing importance in silts, but still measurable in sands (see Schmertmann 1976, Figs. 11 and 28), and with the importance generally increasing with the log of a decreasing d_{10}. A related discussion in Section **12.2** shows that the time needed for secondary consolidation increases with Φ'_α.

9.3 Explanation of Φ'_β

Terzaghi et. al. (1996, p. 147) describe, as have others, a soil's frictional shear resistance Φ' as the sum of a particle/particle sliding component Φ'_μ, and a geometrical interference component Φ'_g, or $\Phi' = \Phi'_\mu + \Phi'_g$. According to the above discussion of Figure 12, the (σ' tan Φ'_α) part of the **I**-component from **IDS**-tests on clays results from AWL particle/particle sliding. Therefore the saturated $\Phi'_\mu = \Phi'_\alpha$. Having previously established under **7. LINKING...** that $\Phi' \approx \Phi'_\alpha + \Phi'_\beta$, **then the geometrical interference component $\Phi'_g \approx \Phi'_\beta$**. As in Figure 7, the writer also describes these Φ'_α and Φ'_β frictional components as "secondary" and "primary".

10. BOND COHESION I_b

In the writer's opinion this paper demonstrates in Section **6**, and in Figures 3, 4 and 6 the existence of a real cohesion in extruded kaolinite clay. It seemed roughly constant with strain between ϵ = 1/2 to 10%. Figure 2 shows the

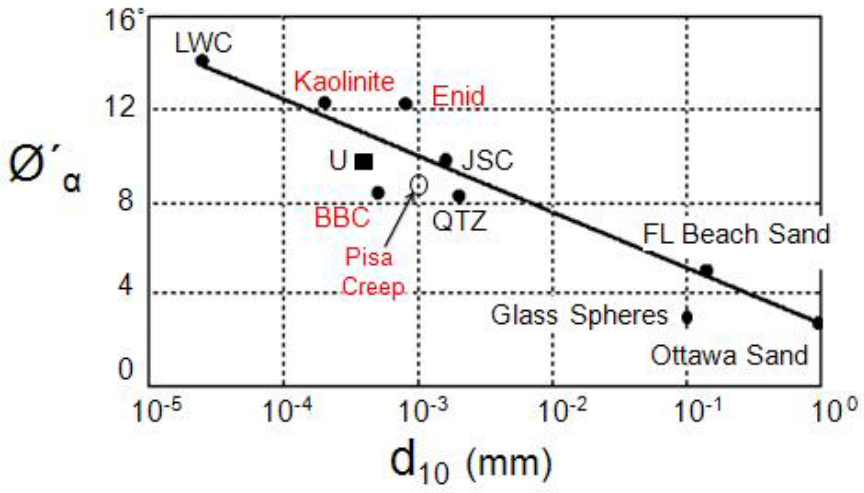

Figure 13: Dependence of Ø´α on d_{10}

same for extruded BBC. Based on the available **IDS-**test data, the strains of extrusion and **IDS**-testing do not destroy the $\mathbf{I}_c$ cohesion. This type of cohesion most likely results from the electrochemical forces of attraction between the clay particles and their AWLs and has a magnitude approximately independent of strain. In this sense it behaves plastically after Є>1/2%.

However, Lambe (1960, Figure 9) and Mitchell (1993, p. 373) detailed at least five different types of cohesion, including the above, with some more easily destroyed by strain. The writer will now present examples of more brittle cohesion than the plastic $\mathbf{I}_c$, resulting from bonding that appears to have developed during testing in the laboratory or from ageing in the field. Denoting such bond cohesion as the "$\mathbf{I}_b$" part of **I**, Equation (4) expresses the total **I**. But, keep in mind that the $\mathbf{I}_\alpha$ part denotes the paradoxical AWL friction and not a cohesion.

$$\mathbf{I} = \mathbf{I}_\alpha + \mathbf{I}_b + \mathbf{I}_c \quad \text{.....(4)}$$

10.1 During Very Low Rates of Shear

A previous discussion of Figure 10(a) in **8.3** noted a measurable decrease in **I** at Є = 1% with a large decrease in $\dot{Є}$. However, at $\dot{Є} \approx 10^{-4}$ %/min a decreasing **I** somewhat abruptly (on a log rate scale) turned to an increase in the next log cycle of strain rate while Φ'_β continued to increase. The writer speculates that in Figure 10(b) the strain rate became so low that the considerable ageing time involved (10^5 min or 70d) allowed measurable $\mathbf{I}_b$ bonds to form, which caused **I** at Є = 1% to increase in this extruded kaolinite.

10.2 From Overconsolidation

Simple, one day isotropic overconsolidation to an OCR = 4 appears sufficient to start the formation of brittle bonds. Figure 14 shows data from **IDS**-tests on extruded specimens of kaolinite and Enid clays. The writer used $\dot{Є} \approx 5x10^{-4}$ %/min to permit the curve hopping procedure at very low strains, which in turn permitted separating the components at these strains. For both OC clays we measured a distinct peak in the otherwise expected smooth trend for the increase of the **I** component with strain. The stippled shading in Figure 14 shows the peaks. It looks like brittle $\mathbf{I}_b$ bonding, that developed during only one day of OC, increased the **I** component over the first approximately 0.1 to 0.2% of **IDS**-test strain.

Note the connection between the postulated development of bonding in kaolinite due to ageing in the **10.1** discussion with the demonstrated bond development in **10.2** due to OC. This evidence supports the possibility of accelerating some ageing effects by OC – and implies the reverse, that ageing could produce OC (subsequently demonstrated in **12.3 AGE-**

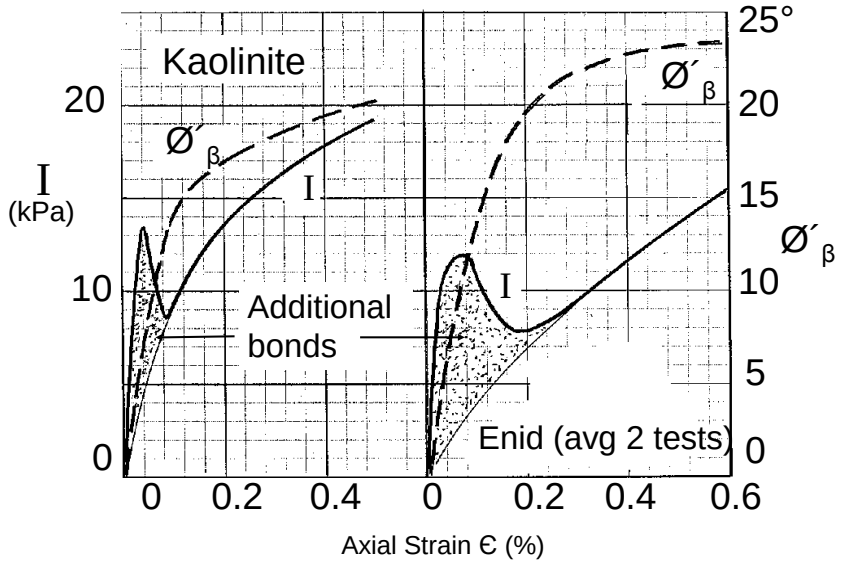

Figure 14: Evidence of Rigid Bonds after 1 day, Isotropic OCR = 4 (σ'_c = 700, σ'_{cu} = 175, σ'_{1h} = 170, σ'_{1l} = 135 kPa)

ING PRECONSOLIDATION). Mitchell (2008) supports the latter possibility for sands, as does Terzaghi (1941b, pp 3,4).

10.3 In Undisturbed Clays

Those $\mathbf{I}_b$ bonds that remain after undisturbed sampling, trimming and handling in a laboratory should show up as additional **I**-component compared to the same clays after severe remolding by machine mixing and extrusion. Comparative **IDS**-tests using specimens from the same undisturbed block of BBC provide an example. The undisturbed e = 0.82 and the machine extruded e = 0.65, both after isotropic NC to σ_c' = 400 kPa. **I** values at ϵ = 1% ≈ 70 and 50 kPa, respectively, indicating an $\mathbf{I}_b \approx 20$ kPa destroyed by the extrusion. That allowed the additional Δe = 0.17 consolidation. For this and other **IDS**-test examples of $\mathbf{I}_b$ cohesion using undisturbed clays see Schmertmann and Osterberg (1960, Figures 21-24), and Schmertmann (1962, Figs. 2, 7, and 1976, Figs. 17-19).

10.4 Terzaghi's Bonding

Terzaghi (1941a, 1941b), based on his prior research studying adsorbed water layer behavior and described in Terzaghi (1920, 1931), and illustrated by him on the left side of Figure 12, thought that adjacent clay particles with enough force+time acting between them would eventually come into solid/solid particle contact and form a 'cold-weld' type of rigid bonding. Then it would take a threshold shear force, or a "critical pressure", to break these bonds. This presents another possible type of cohesion, now included in $\mathbf{I}_b$, which also seems consistent with the low-strain, brittle bonds measured by the **IDS**-tests discussed above. See 12.10.3.2 for further discussion of "critical pressure".

11. THE SHEAR COMPONENTS

As developed in this paper, the shear components consist of cohesions that produce a tensile strength plus the Φ'_α and ($\Phi'' \approx \Phi'_\beta$) friction components. The following, starting with cohesion, gives the writer's opinions, based mostly on this research, as to the physical basis for each of the components.

11.1 $\mathbf{I}_c$ Cohesion

In the case of severely remolded clays, such as when machine-extruded, a plastic "$\mathbf{I}_c$" cohesion probably results from the net attractive forces between the surfaces of the particles in near-contact but still separated by adsorbed water layers. It mobilizes rapidly within a compressive strain of 1.0% or less and appears slightly strain rate dependent, as discussed below in **11.2**.

11.2 $\mathbf{I}_c$ Reliability

An issue in geotechnical engineering involves the question of the reliability in practice of $\mathbf{I}_c$ cohesion in natural clays. Critical State Soil Mechanics does not use cohesion in "fully softened" clay because of its supposed unreliability. The research results described herein suggest a complicated but ultimately reliable $\mathbf{I}_c$ in undisturbed clays, partly because of compensating time-transfer effects.

If $\mathbf{I}_c$ cohesion results from the behavior of the AWL, as the writer postulates, then it might exhibit viscous strain rate effects and reduce to zero at very low strain rates. In part to check this, Strømann (1971, pp. 97-103) performed drained, compression, relaxation tests on three extruded, OCR = 2, kaolinite specimens from the same source as the kaolinite used for the **IDS-**tests in Figures 3 and 4. She followed an approximate constant structure Mohr envelope (CSME, see Schmertmann, 1976 pp. 65-66, 78) backwards to a very low effective stress and, by a short extrapolation, obtained an $\mathbf{I}_o$ cohesion (her notation) intercept with the $\sigma' = 0$ axis. The final relaxation drained creep rates of compressive strain that applied to these CSMEs dropped $\dot{\epsilon}$ to less than 1.27×10^{-5} %/min, or more than 55 days/%, by an unknown amount. However, she determined still measurable values of $\mathbf{I}_o$ from 1.0 to 4.8 kPa at $\epsilon \approx 0.9$ to 3.8%.

The above compares with the aforementioned approximate range for $\mathbf{I}_c$ of 7-12 kPa obtained from **IDS-**tests using an average $\dot{\epsilon} \approx 7 \times 10^{-3}$ %/min, or more than 500 times faster. The cohesion reported herein for ex-

truded kaolinite may reduce with reduced strain rate, but, if so, it does so very gradually. We need more experimentation to determine if it can reduce to zero.

It thus appears that $\mathbf{I}_c$ might or might not eventually drop to zero and lose its contribution to the total mobilized shear resistance. But that does not consider the associated time-transfer increase in the **D**-component, σ' tan Φ'_β, which can more than compensate for the loss in $\mathbf{I}_c$ as discussed under **8.1 Undrained Creep** and **8.5 Anisotropic Consolidation**. In addition, any increasing strain and strain rate resulting from an increased loading will rapidly remobilize the AWL-based $\mathbf{I}_\alpha$, and presumably also any lost $\mathbf{I}_c$, producing a stronger clay during this next interval of strain.

Note that if $\mathbf{I}_c$ does reduce with time to zero or near-zero, this change becomes part of the Φ'_α viscous secondary shear behavior shown with a "?" in Figure 7 and discussed in **12.2**.

11.3 $\mathbf{I}_b$ Cohesion

Other types of cohesion behave in a more brittle fashion and with more permanence. For example one can have pressure-induced and/or chemically-induced precipitation and cementation. These effects usually increase with the time allowed for them to develop. This paper has shown in Figures 10 and 14 how they may develop even during laboratory testing times in severely remolded (extruded) clays or, perhaps they develop quickly because of the prior severe remolding. The writer refers to them as "bond cohesion", denotes them by "$\mathbf{I}_b$", and by references provides examples of $\mathbf{I}_b$ in several undisturbed clays.

11.4 $\mathbf{\Phi'_\alpha}$ Friction

The writer has shown that this particle/particle sliding friction could, and likely does, result from the particle surface lubrication effects of the viscous adsorbed water layers on the surfaces of all particles, but particularly important on the fine particles of layer-lattice minerals (phyllosilicates) in clays. All of the following findings, from mostly strain-controlled **IDS**-tests using extruded clays, seem consistent with this finding about Φ'_α:

11.4.1 Φ'_α mobilizes rapidly and then decreases gradually with axial strain in extruded clays.

11.4.2 Φ'_α has approximately the same magnitude over ϵ = 0.5 to 10% in extruded clays, and in this sense behaves plastically.

11.4.3 Φ'_α has a magnitude very similar to that reported from research determining the saturated, sliding friction of some phyllosilicates typical in clays.

11.4.4 Φ'_α has a similar magnitude when tested in compression and extension**.**

11.4.5 AWL effects and a viscous Φ'_α friction provide an explanation for the apparent paradox with a σ' = 0 'nominal cohesion' intercept in an **IDS**-test.

11.4.6 Φ'_α appears approximately independent of void ratio, OCR, secondary compression time, dilatancy and interlocking, deflocculation or dispersion, clay mineralogy**,** isotropic or anisotropic consolidation, and the stress-time path for consolidation (see Schmertmann 1976, Tables 1-4a).

11.4.7 A viscous creep behavior of the AWLs would explain the transient and "secondary" behavior of Φ'_α.

11.4.8 Φ'_α behaves as the sliding friction Φ'_μ in Terzaghi et. al. (1996, p. 147).

11.4.9 Φ'_α usually decreases with an increase in particle size.

11.5 $\mathbf{\Phi'_\beta}$ Friction

The writer believes (also in Schmertmann, 1976, p. 91), as do Terzaghi et. al. (1996, p. 147) and probably many others, that this component of clay friction, which the 1996 reference denotes as $\Phi'g$, results from particle, and/or aggregates of particles, geometrical interference effects, including locking and unlocking, rotations, bending and unbending, and breaking or other damage. All of the following findings seem consistent with this description of Φ'_β:

11.5.1 Each **IDS**-test directly measures a primary clay friction Φ'', or approximately Φ'_β, versus axial strain.

11.5.2 Φ'_β increases gradually with compressive strain in NC clays, and more rapidly as the OCR of an extruded clay increases.

11.5.3 At a given strain Φ'_β increases with increases in interlocking and positive dilatancy .

11.5.4 At a given strain Φ'_β increases with the void ratio reduction resulting from overconsolidation.

11.5.5 At a given strain Φ'_β increases due to a time transfer from the transient Φ'_α in stress controlled testing. This demonstrates its stability versus Φ'_α.

11.5.6 At a given compressive strain after anisotropic consolidation, Φ'_β increases with increasing the $(\sigma'_1/\sigma'_3)_c$ ratio.

11.6 Φ'_β versus Φ'_α Reliability

This paper includes some examples of the time transfer of the particle/particle AWL sliding Φ'_α to the more stable particle interference Φ'_β. The cited references have more examples. Testing with strain control continually mobilizes almost all the AWL-controlled Φ'_α. But, this highly viscous Φ'_α may creep to near-zero under constant-load time in the field. This sliding creep will likely produce more geometrical interference between particles and increase Φ'_β. If not, as with residual strain conditions, the clay will become overloaded compared to its strain controlled test strength and respond with continuing creep, some form of structural collapse, or otherwise fail. Note, as shown for example by Figure 9(b), that Φ'_β can increase by suitable cycles of load increase and rest at constant load, but presumably only to some maximum capability, $\Phi'_{\beta max}$, controlled by its current structure. See **12.1** for more discussion of this presumption.

11.7 Summary Equation

The following equation (5) summarizes the Mohr-Coulomb envelope components developed from the writer's interpretation of the research results described herein. The same equation (5) introduced Section **2. SUMMARY OF THE IDS-TEST** with a preview of the interpreted shear components, together with an introductory description of the components.

$$\{\tau = \mathbf{I}_c + \mathbf{I}_b + \sigma' \tan [\Phi'_\alpha + (\Phi'_\beta \approx \Phi'')]\}_{\epsilon,t} \quad (5)$$

12. PRACTICAL CONCEPTS

If the research results and new or refined concepts herein add to the fundamental engineering understanding of soil and clay behavior, then they should find applications in both research and practice, perhaps in the form of adjustments in how engineers assign the causes of and test and model the engineering behavior of clays. The following presents thirteen example concepts and possible adjustments to illustrate the practical potential. They add to the **IDS**-test itself, which makes it practical to identify the M-C shear components in clay.

12.1 Residual $\Phi' \approx \Phi'_\alpha$

At residual strains the particles have, by definition, a minimum of bonding and of interlocking and other particle/particle geometrical interference. That suggests $\mathbf{I}_b$ and Φ'_β might then have only small values. That leads to the possibility that AWL effects might dominate the frictional shear resistance at $\Phi'_{residual}$ and hence Φ'_α might dominate at residual strains in clays. Figure 15 provides data that supports this possibility.

In a discussion Hamel (2004) provided some laboratory test and field back-calculated $\Phi'_{residual}$ versus PI values from colluvial landslides in Pennsylvania. Figure 15 shows his laboratory $\Phi'_{residual}$ test points and the matching range of $\Phi'_{residual}$ from the landslides. The writer has superposed on these data the Φ'_α values available to him from extruded clays within the PI range plotted, including the Φ'_α results from undrained **IDS**-tests using undisturbed specimens from three soft clays—see Schmertmann (1976, Figs. 17-19). The similarity between the two sets of values, $\Phi'_{residual}$ and Φ'_α, shows that the viscous Φ'_α friction shear behavior of the adsorbed water layer may provide a major part of the total residual shear resistance of at least some clays.

Since the initial preparation of Figure 15 the writer has encountered other field and lab residual strength data, now added into Figure 15, that continues to support the possibility that $\mathbf{I}_c$ (or c′) and Φ'_α from AWLs provide a major part of residual strength. Tiwari et. al (2005) studied 6 landslides in Japan's Nigata prefecture that failed along slickensides in an OC clay with a PI range of 31 to 68%, averaging 47%. Backfiguring using a Japanese method gave average c'_{res} = 7.7 kPa and Φ'_{res} = 10.4°. Eighteen lab ring shear tests on undisturbed and remolded specimens gave similar results, with an overall average c'_{res} = 4.0 kPa and Φ'_{res} = 12.1°. In addition, Failmetzger and Bullock (2008) reported an insitu Iowa borehole shear test that gave values of c'_{res} = 8.8 kPa and Φ'_{res} = 11.2° in an OC clay with a PI ≈ 24%. Smith et. al. (2006) reported that the OC, slickensided, marine, stiff clays of the Potomac Group Formation underlying parts of Washington D.C. and Baltimore had residual strengths of Φ'_{res} = 10 to 15° (using c'_{res} = 0) and a typical PI ≈ 50%. The above additional data support the initial data in Figure 15.

In further addition, comments and data found in the NGI's 1967 Conference Proceedings seem to reinforce the possibility that $\Phi'_{residual} \approx$ the **IDS**-test-determined Φ'_α. Morgenstern (1967) wrote "It seems possible that the physical basis for the low residual strength exhibited by most clays resides in basal shear plane shear of the platy particles." Hutchinson (1967) noted that field determinations of $\Phi'_{residual}$ in inland slopes of London clay varied from 8°-10° with PIs from 20-28%. Figure 15 includes a box showing these ranges, which fits within the previous data shown. Kenney (1967a) concluded that $\Phi'_{residual}$ does not depend on clay plasticity (as in Figure 15) but does depend on the attractive forces between particles. In Kenney (1967b) he strongly recommended using the **IDS**-test for studying the fundamental strength behavior of clays.

From all the above data it seems possible that the cohesion and friction shear components of the AWL can logically and quantitatively account for much of the residual strength of many clays if bonding and the particle interference friction Φ'_β reduce to small values at residual strains.

However, the above possibility presents the writer with an as yet unresolved mystery. Other Φ'_β component behavior from this research appears to provide counter evidence, namely that time and continuous strain, over the interval of *c.* 1% to the maximum 10% investigated, decreases Φ'_α and increases Φ'_β. One possible resolution involves the progressive destructuring of a clay with Φ'_β reducing to a low $\Phi'_{\beta max}$ capability at higher residual strains, as discussed below.

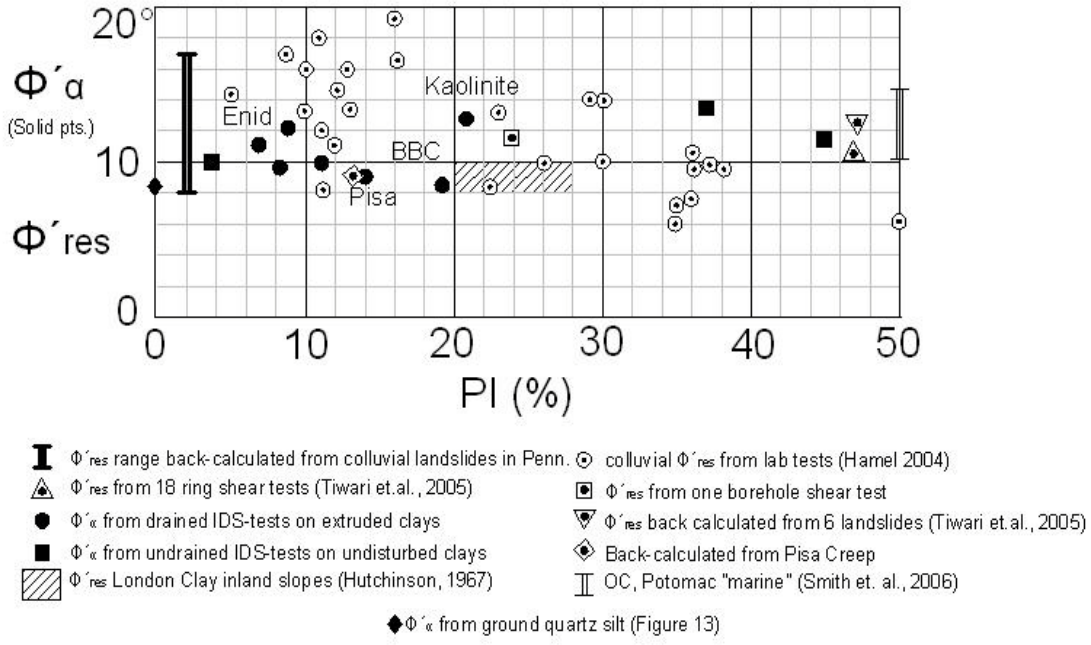

Figure 15: Evidence that $Ø'_\alpha \approx Ø'_{residual}$

Consider a stable clay slope loaded to a just-beginning creep condition with Φ'_{β} fully mobilized at the clay's current structures' $\Phi'_{\beta max}$ capability. For whatever reason the shear load on the slope increases and it begins to creep with viscous Φ'_{α} partially mobilizing as required. The additional strain causes the clay to destructure a little and $\Phi'_{\beta max}$ reduces. The next cycle of shear load increase and destructuring reduces $\Phi'_{\beta max}$ a little more and mobilizes a little more Φ'_{α}, and the viscous creep rate increases. After more such cycles $\Phi'_{\beta max}$ has reached its destructured minimum of particle geometrical interference and the viscous Φ_{α} has mobilized almost fully. Thus, the shear resistance to slope movement now becomes primarily due to the unstable, viscous AWL Φ'_{α} and c' with $\Phi'_{\beta max}$ at its current lowest possible value. The next cycle of load increase increases Φ'_{α} to its maximum value with no more Φ'_{β} to transfer to and serious creep begins. Thus, $\Phi'_{residual}$ might $\approx \Phi'_{\alpha}$.

Note that the above scenario resembles the cyclic, progressive destructuring of OC clay slopes described by Bjerrum (1967b) as due to the progressive breaking of bonds. Instead of the breaking of bonds the above scenario has progressive destructuring that reduces $\Phi'_{\beta max}$, and may or may not include breaking bonds.

Discussion of the pro and con evidence of the above scenario falls beyond the scope of this paper. However, one especially interesting piece of pro evidence concerns the reported creep of the upper sandy and clayey silt layer under the Pisa Tower (Burland et. al. (2009)). The writer made a rough calculation of the average operational effective friction angle on the authors-identified, spherical rotational failure surface during the last 50 years of creep and obtained $\Phi'_{creep} \approx \Phi'_{residual} \approx 9°$. The writer estimated from the data available to him that the silt layer has a PI ≈ 13% and a $d_{10} \approx 10^{-3}$mm. These Pisa soil data fit well within Figures 13 and 15 herein and suggest that Φ'_{creep} may also have a major Φ'_{α} component at the estimated (assuming simple shear over a 100mm thick shear zone) equivalent $\dot{\epsilon} \approx 2x10^{-6}$%/min creep rate for this tower's rotation.

12.2 Secondary Consolidation and Secondary Shear

During the effective stress and volume changes that define consolidation, the relatively incompressible solid particles, and/or aggregates of particles, must change their positions to accommodate the consolidation. The sum of all the mobilized shear resistance within a clay's structure must resist and eventually match the additional shear applied as the volume change gradually ends. The writer assumes that the internal shear resistance of a clay's structure determines its consolidation behavior, not the reverse. If we have "secondary consolidation" then we must have "secondary shear". This research clearly identifies this secondary shear, as follows:

As illustrated in Figures 1b,c and 7, Φ'' (or Φ'_{β}) results from the rapid shear mobilization response to an effective stress change – much like primary consolidation results from a rapid void ratio reduction response to an effective stress increase. Then, a generally much slower, delayed response occurs as the viscous Φ'_{α} friction reduces, or continues to reduce, as it transfers and adds to the more stable Φ'_{β} friction. It might help understanding to think of the above transfer as a "secondary shear" frictional resistance that adds to the "primary shear" available to resist the next consolidation load increase. Figure 7 illustrates how this transfer develops a larger total $\Phi' = \Phi'_{\beta} \approx (\Phi'_{\alpha} + \Phi'')$ frictional shear resistance at the time when the clay structure has completed this secondary shear transfer process to $\Phi'_{\alpha} = 0$.

According to the above and previous explanations of Φ'_{α} friction resulting from viscous AWL behavior, the time decay of mobilized secondary shear and its slow transfer to primary shear (Φ'_{α} transfers to Φ'_{β}) produces the secondary consolidation during the transfer search for stability. **IDS-**tests after secondary can capture the increase in Φ'_{β}. For example, Schmertmann (1976, Figure 9), (1982, Figure 8) or (1991, Figure 30), showed that progressively increasing the isotropic secondary consolidation time from 85 to 50,000 minutes increased Φ''(or Φ'_{β}) progressively from 1.2° to 6.9° at ϵ = 0.5% in **IDS**-tests on kaolinite.

More evidence comes from the similarity between the $(\Phi'_{\alpha}/\Phi'_{\beta}$ and (C_{α}/C_c) ratios from

clays, silts, and sands. Again according to the above and simplifying for clarity, the primary Φ'_β controls the primary consolidation and C_c and the secondary Φ'_α controls the secondary consolidation and C_α . From many studies, most by G. Mesri and his students, the (C_α/C_c) ratios for inorganic soils typically vary between 0.01 in granular soils to 0.05 in silts and clays (Terzaghi et. al. 1996, p. 110). The (Φ'_α/Φ'_β) ratios typically vary from *c.* (3°/30°) = 0.1 in granular soils to *c.* (10°/20°) = 0.5 in silts and clays (Figs. 7, 8, 13). Thus, each of the ratios vary by a factor of *c.* 5 going from granular to clays. This similarity provides further evidence that the shear components developed herein help explain both primary and secondary normal consolidation behavior.

Terzaghi (1941b) described secondary consolidation as *"…the gradual displacement of the viscous portion of the adsorbed water films…"*, which he then called the *"process of solidification"*. He wrote further that *"…the time required for reaching a given degree of solidification increases with the reciprocal of the square of the grain size."* One can then also say the time increases linearly with the negative value of the log of grain size – as does Φ'_α in Figure 13. We thus have another connection between Φ'_α and secondary consolidation. It suggests that secondary time increases exponentially with Φ'_α, which checks qualitatively with experience.

The present research results also provide evidence related to any remaining controversy about whether or not primary and secondary consolidation occur **(A)** with no secondary during primary or **(B)** secondary also occurs during primary. Many researchers believed **B** correct. For example: Terzaghi (1941b) also wrote that *"Both field and laboratory experience demonstrates that we have to deal almost exclusively with the second case* **(B)***."* Taylor (1942, pp. 65, 136; 1948, p. 243) investigated the **(A)** and **(B)** hypotheses in detail and agreed with **(B)** and the need to include a "plastic structural resistance to compression" throughout the consolidation. Forty-eight years later Leroueil (1996, p. 538) also investigated both and presented data that support his conclusion for **(B)** and also states that *"Hypothesis **(B)** assumes some sort of 'structural viscosity'…"*. Sixteen more years later this paper demonstrates that the AWL's viscous cohesive $\mathbf{I}_c$ and frictional Φ'_α secondary shear components supply this "plastic structural resistance to compression" or 'structural viscosity' and the writer also supports **(B)**.

12.3 Ageing Preconsolidation

12.3.1 Decreasing Rate of Consolidation Loading

As discussed above and shown under the **8.4 Secondary Compression** and **8.5 Anisotropic Consolidation**, time and drained shear+ time can stiffen and strengthen a clay's structure by increasing the **D-**component. It then seemed reasonable to expect that allowing more time for a given effective stress consolidation increase, **when stress controlled with rest times**, could allow time for the **D**-component to increase, the structure to stiffen, and perhaps then the consolidation volume change would reduce versus that with a greater effective stress loading rate. To check this, the writer performed some comparative isotropic consolidation tests with greatly reduced rates of effective stress increase. As shown in Figure 16, decreasing the rate of NC loading in two non-swelling clays did reduce the consolidation volume change due to an isotropic effective stress increase from 100 to 350 kPa. However, it did not happen for the expected reason. The formation of bonds appears to have interfered, as explained below under 12.3.2.

Each of the points in Figure 16 represents a separate test of the isotropic, normal consolidation of a duplicate specimen of extruded, reconstituted kaolinite and the natural Enid residual clay. The writer achieved the greater than 1.0 day times by very small increment≈(constant) or 10-increment loading, both with rest periods. Both methods produced about the same reduced void ratio change.

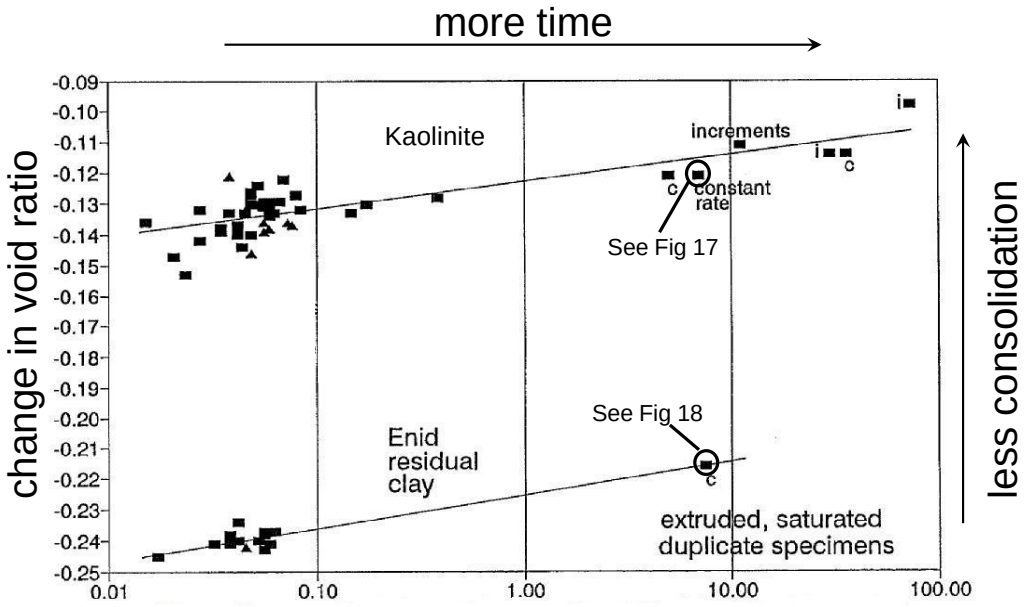

Figure 16: Examples of Decreasing Volume Change by Increasing the NC Time to σ'_c

12.3.2 Components after low rates of consolidation

Consider the two, circled 7-day consolidation time points in Figure 16. For each of these, at the end of the consolidation time, the writer performed an **IDS**-test to separate the components and compare them with duplicate specimens with only approximately one hour of primary consolidation time over the same effective stress interval. Figure 17 shows the results from kaolinite and Figure 18 from the Enid clay, both extruded. Both comparisons produced similar results. The 7-day **I**-component increased and then decreased over a 3% compressive strain interval while the **D**-component (Φ'_β) decreased.

Figures 17 and 18 do not show the aforementioned expected increase in Φ'_β. Instead, Φ'_β decreased. Nevertheless, the consolidation void ratio change did decrease with increasing the time to accomplish the effective stress increase. It appears that each clay's increased resistance to volume change resulted from the addition of cohesive bonding, $\mathbf{I}_b$, as shown by an increase in the **I** component. Then one might also predict that Young's modulus, E, would also increase in the 7-day versus the 1-hr **IDS**-tests because of the rigidity expected from cohesive bonds, as shown in Figure 14.

A check of the $\sigma_1'_{high}$ stress-strain curves showed that E did increase approximately 65% when measured linearly between successive data points over the (σ'_1-σ'_3) stress range of approximately 400 to 800 kPa, all with $\epsilon \leq 0.1\%$. The E for kaolinite increased from 900 to 1580 kPa, and for the Enid clay from 1300 to 2060 kPa, despite the low-strain reduction in Φ'_β and the reduced consolidation (greater void ratio) after the 7 day versus 1 hour time to apply the effective stress increase.

The writer now has six measured behaviors which all support that the formation of $\mathbf{I}_b$ cohesive bonds very likely caused the reduced consolidation with increased time, namely:

12.3.2.1 **I** increased
12.3.2.2 Φ'_β decreased
12.3.2.3 E increased
12.3.2.4 $\mathbf{I}_b$ bonds can develop in the lab at $\epsilon = 0.1\%$
12.3.2.5 The bonds inhibited the strain mobilization of the particle interference Φ'_β
12.3.2.6 3% additional axial strain destroyed $\mathbf{I}_b$.

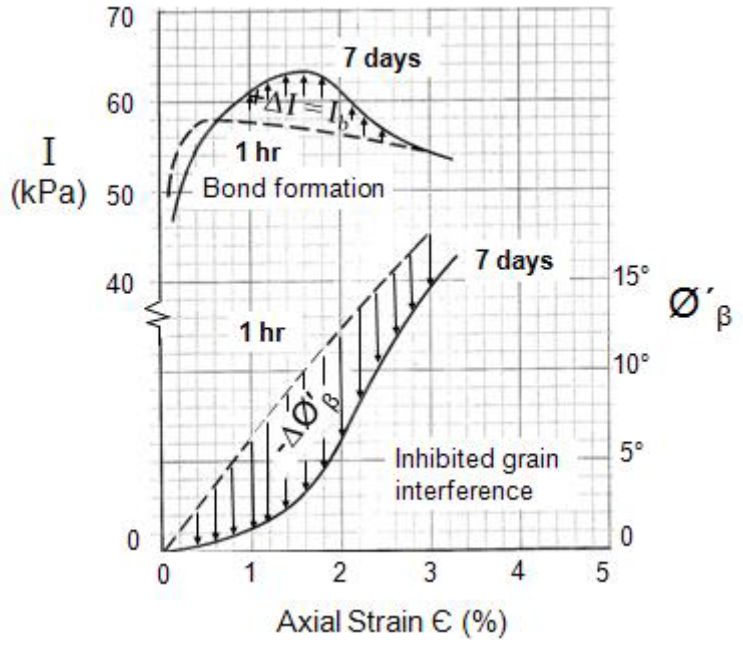

Figure 17 Extruded Kaolinite, 7 days versus 1h for σ'_c Effective Stress Increase from 100-350 kPa

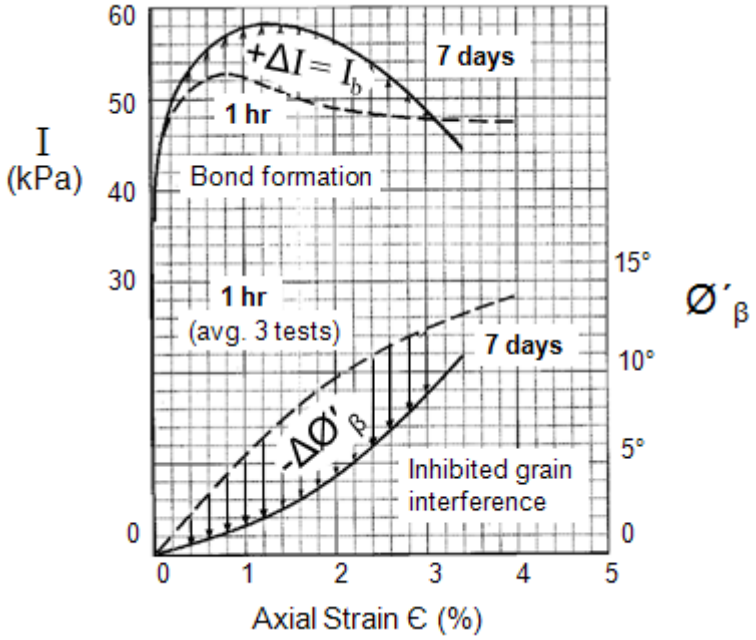

Figure 18: Extruded Enid Clay, 7 days versus 1h for σ'_c Effective Stress Increase from 100-350 kPa

12.3.3 Reliable Ageing Preconsolidation

All the consolidation theories known to the writer, with one important exception, and however they separate and then add primary and secondary consolidation effects, and with whatever load increments used, ***predict more total consolidation with more total time for the effective stress transfer***. Figure 16 shows a counter-intuitive **less** consolidation with **more** time. Terzaghi (1941a) provided the exception. Taylor (1942, pp. 77, 137; 1948 p. 246) supported the exception by also noting that the development of bonds during long sedimentation times would reduce volume change. As described above, bonds did reduce volume change in the lab tests of extruded kaolinite and Enid clay. Terzaghi also provided examples

of the consequences – including almost constant void ratio versus depth profiles in natural, uniform NC clay layers deposited over long periods of time. The writer has found similar profiles in the literature, for example in Landva et. al. (1988) in a clayey silt and in two sensitive Norwegian clays in Lacasse et. al. (1985, Figs. 2, 3) or Burland (1990, Fig. 32), and in Mitchell (1976, Fig. 11.18) (1993, Fig. 11.18).

Terzaghi (1941a) also showed how an ageing preconsolidation or overconsolidation effect would reduce the settlement of real foundations. His Figure 7, partly reproduced as Figure 19, shows **schematically** a sedimentation compression curve "C_s", the real foundation settlement curve without prior excavation, "C", and the consolidation test curve "C_u". The rate of loading increases dramatically from C_s to C to C_u. He showed that he would expect an effective overconsolidation in an otherwise NC deposit, which the writer has labeled the "ageing p_{ca}".

The Bjerrum (1967a, Figures 14-18, 1972, 1973) secondary consolidation creep and quasi-preconsolidation model predicts the ageing preconsolidation, but also that it will eventually disappear with creep. But he also noted (1967a, p. 108), that bonding could slow or stop the secondary creep. Indeed, engineers have successfully used this ageing effect innumerable times in practice to permit the use of shallow foundations with loads below the ageing p_{ca}. Landva et. al. (1988) provided a well documented example for a 9 storey bank building over uniform, sensitive, NC, clayey silt with an average PI ≈ 10%. Schmertmann (1991, pp. 1289-93) also noted the practical use of p_{ca} by engineers in New Orleans, Baton Rouge, Bangkok, and Porto Tolle (also see Schmertmann (2003)). Duncan et. al. (1991) discussed another reliable p_{ca} example with San Francisco Bay clays. Ellstein (1992) noted a reliable p_{ca} in Mexico City clays for 1 and 2 storey construction, but not for 3. Low et. al. (2008) provided a recent example of $(p_{ca} + p_o)/p_o \approx 3$ in a Singapore clay. Clyde Baker (2009, personal communication) reported routinely using p_{ca} in Chicago clays. Typical values of $(p_{ca} + p_o)/p_o$ = 1.25 to 2 in practice. They usually increase in oedometer tests with the quality of the sampling of the clay.

The shear-time Φ'_α to Φ'_β transfer behavior of the AWL and/or the formation of bonds during natural sedimentation rates of loading permit a reliable p_{ca} to develop in many geologically NC clays. Leonards (1972) strongly agreed about reliability. Also see Leroueil (1996, p. 536) and Section **12.10.3** for further agreement.

12.4 Applicability to Silts, Sands, and Partial Saturation

The research and concepts developed herein focused on the engineering shear behavior of saturated clays. But, the writer also found that

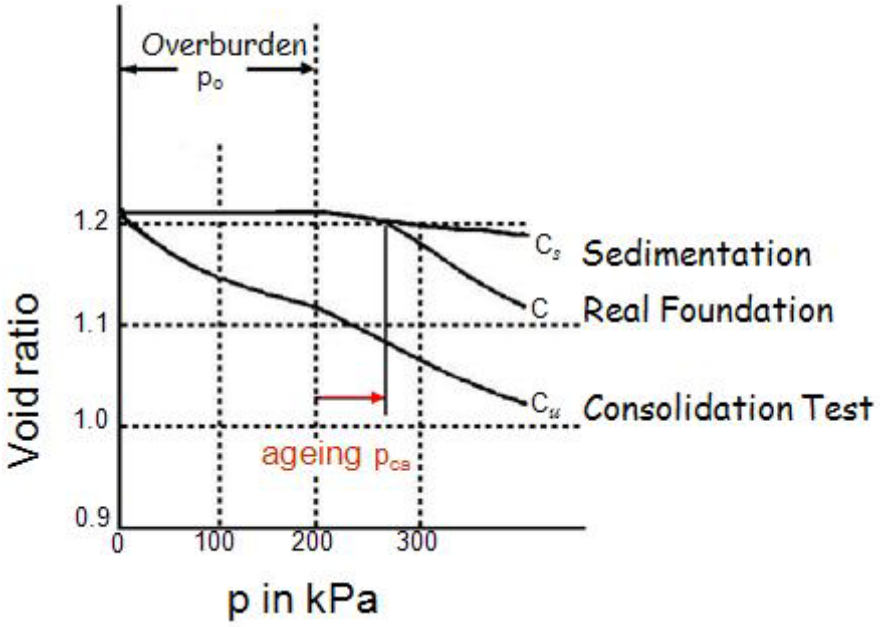

Figure 19: Ageing Preconsolidation p_{ca} from Terzaghi (1941a)

these concepts may apply to many saturated, particulate soils. All such particles have surfaces in contact with a fluid, generally water, with which they interact to form a boundary layer such as the AWL with clays. This layer will have properties different than the truly dry surface of the particle or of pure water and influence any soil's mobilization of its shear resistance components.

Silts, sands and even glass spheres have a measurable Φ'_{α}-component in **IDS**-tests. Plotting the artificial ground quartz silt with a PI = 0, from Figure 13 into Figure 15 suggests that Φ'_{α} has a minor dependence on PI that extends to non-plastic silt and sand, and even to glass spheres. Figure 13 shows a natural sand and an artificial Ottawa sand with Φ'_{α} values of about 5° and 3°, respectively. Schmertmann (1976, Figures 11, 28) provides data from these sand tests.

As noted in **12.2**, granular soils to clays have similar ($\Phi'_{\alpha}/\Phi'_{\beta}$) shear and ($C_{\alpha}/C_c$) consolidation ratios. This similarity also provides evidence of the importance of the shear components, in particular the viscous Φ'_{α}, in all mineral soils.

Silt and sand soils also develop ageing effects, including an ageing p_{ca}. As noted in 12.3.3, Landva et.al. (1988) reported an important p_{ca} in the Fredericton N.B. clayey silts. Mitchell (2008) noted the continuing enigma of various ageing effects in sands. Schmertmann (1991, Figure 6) showed a p_{ca} after one day of ageing under a plate load test on 'dry' sand in a humid laboratory. Such ageing effects involve changes in the shear resistance components, as discussed in **12.3**.

All the above suggests to the writer that a better understanding of the strain and time effects associated with AWL behavior has the potential to resolve questions about the mobilized shear components of soils other than clay. Terzaghi (1941b, p. 3) had similar thoughts.

More detailed data from silt and sands in Schmertmann (1976, Fig. 11) comes from a combination of tests on saturated, partially saturated, and lab air dried specimens. All saturation conditions produced approximately the same Φ'_{α}. This in turn, suggests the possibility that a sufficient AWL exists to develop Φ'_{α} at all these saturation conditions and that a secondary, viscous, transient shear friction component also forms a part of partially saturated soil mechanics. Various particle/particle attractive forces such as capillary and osmotic pressure provide an additional effective cohesion, as shown in Figure 15 in the reference. The concepts developed herein applied to partially saturated soils seems like a fruitful area for more research.

12.5 Undrained Shear Strength, s_u

A paper by Lunne et. al. (1997) included stress-strain data from 8 CAUC tests (K_o consolidated, undrained triaxial compression with back pressure, and a constant rate of strain) by the NGI on block samples of five low to medium PI Norwegian clays. They produced a common response of a pronounced peak at s_u at compressive strains that ranged from only 0.2 to 1.1%, averaging 0.5%, followed by a steep and then gradually reducing shear resistance with increasing strain. The 6 effective stress paths included in the paper all showed a pseudo-elastic, low dialtancy path to s_u.

The research described herein shows that at ϵ=0.5% the **I**-component has reached, or almost reached, its maximum value while the **D**-component (Φ'_{β}) remains relatively minor, especially if cohesive bonding inhibits its mobilization as in Figures 17 and 18. The undrained strength at ϵ=0.5% or less when neglectingΦ'_{β} then consists of plastic $\mathbf{I}_c$ and brittle $\mathbf{I}_b$ cohesions plus a viscous $\mathbf{I}_{\alpha}$ friction.

The pronounced peak at s_u suggests important $\mathbf{I}_b$ bonding. $\mathbf{I}_c$ and $\mathbf{I}_{\alpha}$ suggest AWL behavior. The bonding seems consistent with a pseudo-elastic and low dilatancy behavior. As shown herein, the AWL components exhibit little or no dilatancy affects, which also seems consistent. Now consider the implications of this for the possible minor importance of effective stress in s_u in these Norwegian clays.

For illustration, say we have a clay that when tested undrained has 1/3 of its s_u from each of $\mathbf{I}_b$, $\mathbf{I}_c$ and $\mathbf{I}_{\alpha}$. By definition, the $\mathbf{I}_b$ and $\mathbf{I}_c$ cohesions do not vary with σ'. The remaining $\mathbf{I}_{\alpha} = \sigma'$ tan Φ'_{α}, which typically $\approx 0.2\sigma'$. Therefore, in this case, effective stress would produce only 0.2/3 = 7% of s_u. It seems possible, perhaps even likely, that effective stress and any changes in pore pressure may have only a minor role in mobilizing s_u insitu at ϵ=0.5% or

less in similar Norwegian clays. This reasoning may apply to many other clays that have developed significant bonding, as during ageing.

The above may also help explain the observation made during testing and research at the NGI (S. Lacasse, 2010, personal communication) of a mysterious, pronounced increase in s_u at very low strain rates compared to expectations of a continuing log decrease in s_u with decreasing strain rate. Perhaps this represents behavior similar to that shown for the extruded kaolinite in Figure 10. Very slow strain rates may provide the time needed for significant bonds to form or for Φ'_β to increase as in secondary consolidation, or both. The resulting increase in shear strength then exceeds the reduction in viscous AWL shear due to the reducing strain rate, and s_u increases.

12.6 Low Strain Modulus and Secondary Shear (G_o and Φ'_α)

Based on three levels of evidence, the writer proposes a direct connection between G_o, residual strength Φ'_{res}, and the AWL viscous friction Φ'_α, as follows:

The first evidence comes from IDS-tests on isotropically NC clays where the **I**-component typically mobilizes five times more rapidly with strain versus the **D**-component. At the very low shear strains used for the dynamic testing for G_o, typically 10^{-3}% or less, the mobilized shear resistance will come mostly from the **I**-component. Recalling that $\mathbf{I} = \mathbf{I}_c + \mathbf{I}_b + \mathbf{I}_\alpha$, only $\mathbf{I}_\alpha$ depends on the effective stress. Because G_o does increase with effective stress as discussed below, this increase comes from $\mathbf{I}_\alpha$ which, as interpreted herein, depends on the viscous behavior of the adsorbed water layer.

Secondly, G_o increases with approximately $(\bar{\sigma}_o)^{0.5}$ (for example see Anderson and Woods, 1976, Figs. 4, 9). These authors included tests on an extruded, saturated ball kaolinite with a PI = 39% and a d_{50} = 0.00025 mm. Using a reference time of t_{ref} = 1000 min, and assuming their $\bar{\sigma}_o \approx \sigma'_t$, the kaolinite's G_o increased approximately linearly with a $\Phi' \approx 18^o$ over their NC $\bar{\sigma}_o$ range of 69 to 275 kPa. This compares with a Figure 13 $\Phi'_\alpha = 12^o$ for an extruded kaolinite with PI = 21% and a d_{50} of 0.001 mm. A rough correction for PI and d_{50} differences would increase the latter Φ'_α value to *c.* 14-15^o. It seems that Φ'_α, and therefore AWL behavior, could account for most of the increasing G_o response to increasing $\bar{\sigma}_o$ in extruded kaolinite and perhaps also in many natural clays.

Thirdly, if G_o in NC clays depends importantly on Φ'_α behavior, then it would have important secondary shear time and temperature effects. The above reference, and many others, document that it does. The N_G term in Eqn. (6) provides a normalized measure of the semi-log increase in G_o (from Schmertmann (1991, p. 1296)) following Δt_{sec} additional time in secondary consolidation after a reference time t_{ref}.

$$\Delta G_o = N_G [\log (t_{ref} + \Delta t_{sec}) - \log t_{ref}] (G_o)_{ref} \quad \text{..... (6)}$$

N_G reduces with the log of grain size from *c.* 0.16 when $d_{50} = 3x10^{-4}$ mm in clay to *c.* 0.02 in sandy gravel with $d_{50} \approx$ 1mm (Anderson and Woods, 1976, Fig. 7; Mesri et. al. 1990, Fig. 1; Schmertmann 1991, Fig. 9). This trend has a striking similarity to Φ'_α versus log d_{10} in Figure 13, and thereby suggests an interdependence between G_o and Φ'_α.

In addition, and as noted in **9. ADSORBED WATER LAYER (AWL)**, temperature changes affect s_u, p_c and C_α. If this results from viscous Φ'_α behavior in the AWL, as postulated, then G_o should also change with temperature. Anderson and Richart (1974) present evidence that it does from test results from 2 artificial and 5 'undisturbed' clays. In one typical example with Detroit clay, G_o increased and decreased 10% when increasing and decreasing the ambient test temperature from 4° to 22°C. The secondary compression drainage also increased and decreased during this temperature increase and decrease. The above further supports the concept that G_o (and secondary compression) depends on a viscous Φ'_α.

From the above attempt to look through the 'fog' of the many variables that can affect G_o to see a bigger picture, it seems the plastic, AWL, $\mathbf{I}_c$ cohesion and $\mathbf{I}_\alpha$ friction provide the "very high viscosity" already used by Terzaghi (1941b, 1955, p. 576) to explain secondary time effects. As described in Section **12.1**, a clay's AWL-controlled behavior also seems to have an important effect on residual strength. It's important effect thus seems to span from the smallest to the largest strains. The writer suggests that the typical semi-log "S" shape of

the entire G versus strain curve obtained from clay, results, at least in part, from the **I**-component behavior of viscous adsorbed water in clays.

12.7 Φ'_β to Understand K_o

12.7.1 K_o Increase During Secondary Consolidation

In Schmertmann (1983) the writer posed the question of what happens to K_o in clay during secondary consolidation. Does it decrease, remain constant, or increase? The experimental data now available shows it slowly increases. Only Soydemir (1984) correctly predicted that K_o would increase during secondary consolidation. He used a mathematical model that included viscosity in the clay's volumetric and deviatoric behavior. The following offers a matching viscous component transfer explanation.

As previously discussed in **12.2**, the secondary part of the consolidation process of a clay's structure adjusting to an increased load involves a time transfer from an unstable Φ'_α to a stable Φ'_β. As developed herein, Φ'_α results from particle/AWL sliding and does not depend on particle interference effects, while Φ'_β does so depend. Despite the one dimensional constraint for the K_o condition, Φ'_α can dissipate with time because of its viscosity. But, a matching increase in Φ'_β cannot fully develop with time because particles, on average, cannot move across, nor can shear strain develop to increase interference along the lateral boundary minor principal plane. This reducing Φ'_α to Φ'_β transfer ability reduces the clay's ability to sustain an increased shear loading and K_o increases with time to maintain equilibrium.

12.7.2 Φ'_β in Jaky's Equation

The writer has some evidence from extruded kaolinite and BBC in Schmertmann and Hall (1961) and Hall (1960) that, when combined with Landva's (2006) work, shows the possible superiority of using $\Phi'' (\approx \Phi'_\beta)$ in Jaky's equation (K_o=1-sin Φ') versus using the current conventional $\Phi' = (\Phi'_\alpha + \Phi'_\beta)$.

Landva reviewed the history and derivation of Jaky's equation, and compared it with Terzaghi's (1943) derivation for K_o when using a friction mobilization factor, and with Mayne and Kulhawy's (1982) empirical correlation data when using Φ'. He concluded that tan Φ' required reduction by a Terzaghi mobilization factor that varied from 0.4 to 1.0, averaging 0.6, to encompass the empirical data. The writer here below suggests the alternative, and gives an example, of using Φ'_β instead of Φ' in Jaky's equation.

From the aforementioned Hall (1961) research the mobilized and maximum values of $\Phi'' \approx \Phi'_\beta$= 12° and 20°, resp., for a mobilization factor = 0.6 at the end of anisotropic K_o consolidation. Using 20° and 0.6 in Figure 4 in Landva's paper gives three correct K_o predictions of 0.63, 0.68 and 0.70. Using a representative Φ'=30° and 0.6 gives a too low K_o=0.50. So does Jaky's equation when using 30°, but it gives a correct 0.66 with 20°. The superior result when using Φ'_β instead of Φ' for estimating insitu K_o seems reasonable because it uses the non-viscous (stable) "primary" Φ'_β friction component for a stable K_o state of stress condition while using Φ' includes the viscous (unstable) "secondary" Φ'_α.

12.8 Normal Consolidation Settlement and the shear components

One of the interesting aspects about "consolidation" concerns the various ways it can occur. They do not lend themselves to a simple definition of the word. For the purpose of this discussion the writer defines "consolidation" as an effective stress increase which may or may not decrease a clay's void ratio and cause settlement. For example, we can have consolidation with and without pore pressure change, as well as pore pressure change with and without consolidation. We can also have "secondary" before "primary" consolidation, instead of the usual reverse. Including the interaction of the mix of the two cohesion ($\mathbf{I}_c$ and $\mathbf{I}_b$) and two friction (Φ'_α and Φ'_β) shear strength components of clay, as described herein, provides an alternative explanation for these different "normal consolidation" (NC) cases.

12.8.1 Classic Terzaghi Case: Consolidation settlement with excess pore pressure (u_e) dissipation

This case involves consolidation settlement due to a load increase of a magnitude sufficient to generate an excess hydrostatic (u_e) pore pressure in the ordinary water phase, which then drains as it dissipates hydrodynamically to near-zero. The resulting volume change produces the settlement.

Bonds, if any, begin to break and a secondary viscous shear Φ'_α mobilizes fully at very low volume and/or shear strain (see **12.10.3**). Additional Φ'_β tries to mobilize by viscous transfer with low strain to the point that it exceeds the current $\Phi'_{\beta crit}$ mobilized during the prior increment of consolidation volume change. The current stable structure then becomes unstable (yields) and compresses and generates the u_e. This u_e dissipates with a resulting reduction in void ratio, which in turn increases particle interference and allows $\Phi'_{\beta crit}$ and Φ'_β to increase. With the dissipation of u_e the rapid, primary consolidation ends, but the total consolidation continues with the viscous secondary consolidation associated with the time transfer of any remaining Φ'_α, adding to the stable Φ'_β. The consolidation stops when the stable Φ'_β and any remaining and/or developing $\mathbf{I}_b$ can carry the increased loading that initiated the current increment of consolidation.

12.8.2 Consolidation with little or no settlement

For the case of total (σ) and effective (σ') loading increasing very slowly, significant u_e may (or may not) develop and dissipate in very small increments that produce only a small total volume change and settlement. The otherwise normally consolidated clay develops an ageing preconsolidation, p_{ca}, as described in **12.3** and reviewed below.

The slow loading increase permits the time for an almost simultaneous, stable structure stiffening to occur due to the Φ'_α to Φ'_β, unstable to stable transfer and/or the formation of new $\mathbf{I}_b$ bonds, or both. Section **12.3** gives an example from lab testing. Referenced constant void ratio versus depth profiles provide examples from the field.

Schmertmann (1991, Figs. 18, 19) and Schmertmann (1993, Fig. 9) also provide examples of u_e dissipation with settlement followed by more dissipation without settlement. Assuming correct measurements, the clay structure must have stiffened and strengthened during the time of prior u_e dissipation and settlement to the point of greatly reducing the settlement with further dissipation. Again, Φ'_α to Φ'_β transfer and/or an increase in $\mathbf{I}_b$ likely provided the stiffening and strengthening. Section 12.10.3 **Lab** provides another example from anisotropic consolidation.

12.8.3 Settlement with no σ'_v increase despite u_e dissipation

Crawford and Burn (1976), Larsson (1986), and others have described settlements of test fills while at constant total loading (σ_v) with the resulting u_e remaining approximately constant instead of reducing. However, consolidation settlement did occur. This can only happen if the clay structure collapses when trying to increase σ'_v, but σ'_v cannot increase because the collapse generates u_e at the same rate that it dissipates. We thus have consolidation with a u_e and ($\beta'_{\Phi crit}$ + $\mathbf{I}_b$) that continually control each other during the continuing void ratio reduction and settlement so as to maintain a near-constant σ'_v.

If one assumes a negligible or a constant ($\mathbf{I}_c$ + $\mathbf{I}_b$) cohesion, the constant shear loading associated with a constant σ'_v must remain in a creeping equilibrium with the mobilized $\sigma' \tan(\Phi'_\alpha + \Phi'_\beta)$ frictional resistance. But, Φ'_β should increase with reduced void ratio and the resulting increase in particle interference effects. Because it does not, Φ'_β must be at a $\Phi'_{\beta crit}$ (yield) condition that reduces due to structural yield at the same rate it would otherwise increase. Hence the counter-intuitive consolidation equilibrium between a constant σ'_v and an increasing settlement.

While “temporary”, the above equilibrium will eventually end with σ'_v increasing. But it can take a long time to do so. Crawford and Burn (1976) provide case examples of 10-20 years of equilibrium duration in sensitive clay.

Note that the above presents a variation of the component transfer and residual creep scenario described at the end of **12.1**. Instead

of the residual shear creep in **12.1** we have a consolidation creep. They could also combine.

12.8.4 Settlement with no σ'_v increase and no u_e dissipation

For the near-zero u_e, constant σ' condition after the essentially complete primary u_e dissipation, secondary settlement continues as the viscous Φ'_α continues to transfer to Φ'_β if Φ'_β has not yet reached $\Phi'_{\beta crit}$. If more Φ'_α remains to transfer, but $\Phi'_{\beta crit}$ has reached a maximum, the secondary creep settlement continues as described above, but with u_e a constant value just above zero. Eventually, the decreasing void ratio may let $\Phi'_{\beta crit}$, and therefore Φ'_β increase, and/or $\mathbf{I}_b$ bonds form and the secondary consolidation stops. If not, it continues at a decreasing rate as progressively more viscous AWL water between the particles gets displaced.

12.8.5 Settlement due to fabric collapse

Engineers have identified various other reasons for the weakening and yielding or collapse of soil fabric, such as vibrations and cyclic loading, particle breakage, mechanical remolding, water and other chemical leaching and solution, internal and external erosion, excavations, and high pore pressures leading to unstable low effective stresses. All of these can weaken and overload the shear resistance of a soil and produce settlement. They can also occur in sequence as in leaching prior to undrained loading followed by high pore pressure and collapse. Many combinations have also occurred. They all have in common a weakening resulting in an overloading that exceeds the soil's current stable ($\mathbf{I}_b$ + σ'tan $\Phi'_{\beta crit}$) shear mobilization capability.

12.9 Burland's Clay Intrinsic Consolidation Line (ICL)

According to Burland (1990, pp. 332-334) his ICL results from the normalized, 1D, incremental normal consolidation of a saturated, reconstituted clay started at a void ratio of 1.25 times the void ratio at the Atterberg liquid limit. At this $1.25e_{LL}$ such a clay has a very low and unstable shear resistance and therefore has both the stable $\mathbf{I}_b$ and Φ'_β components near zero. For the reconstituted clays he and others investigated, Burland reported the ICL independent of the starting void ratio in the range of 1.0 to $1.5e_{LL}$ and the time in secondary compression. He also noted that the water used to prepare the reconstituted clay should have the same chemistry as its natural water. All this suggests significant AWL behavior.

That many reconstituted clays closely follow a normalized ICL line may result from the similar plastic $\mathbf{I}_c$ and Φ'_α AWL viscous shear component behaviors in many clays [see Figure 11 in Schmertmann (1976)]. Comparing the consolidation of natural clays to the ICL can then show how the stable Φ'_β and $\mathbf{I}_b$ components change the ICL position of natural clays versus a reconstituted ICL.

12.10 Minimum Surcharge Ratio for drainage aids to reduce settlement time

12.10.1 Objective

The writer herein defines a surcharge ratio R_s at any depth z in a NC clay as [(the σ'_{vo} vertical effective stress before the surcharge + the $\Delta\sigma_{vs}$ added by the surcharge)/(σ'_{vo})]. Then:

$$R_s = (\sigma'_{vo} + \Delta\sigma_{vs})/\sigma'_{vo} \quad \text{..... (7)}$$

Adding and later removing a surcharge produces overconsolidation in otherwise NC clays. As shown throughout the paper, and illustrated in the schematic Figure 8, overconsolidation increases the subsequent strain rate mobilization of the stable Φ'_β and/or $\mathbf{I}_b$ components. To accomplish this the surcharge must produce enough additional bonds to increase $\mathbf{I}_b$, and/or the strain to increase particle interference to the required increased level of Φ'_β. Using surcharge ratios that cause structural yielding and the generation of u_e also requires the dissipation of that u_e. **However, drainage aids will not help significantly with a too low surcharge ratio because the Φ'_α to Φ'_β transfer occurs because of a highly viscous AWL flow at very low hydraulic gradients instead of a hydrodynamic pore pressure dissipation of low viscosity (ordinary) water at high gradients.** The following attempts to answer the question of

what minimum R_s must one exceed to make drainage aids effective?

12.10.2 A theory for the minimum R_s

12.10.2.1 Normally Consolidated (NC) Case

In Figure 20 the writer presents a sequence of simplified effective stress paths (ESPs) in (p′-q) Mohr coordinates to explain the derivation of subsequent Equation (8). Point "A" shows the (p′-q) location of a NC clay before surcharging with $\Delta\sigma_v$. Placing the surcharge begins to mobilize the additional q required for eventual stability at point "C" for the illustrated R_s = 2. The dormant **I** component, = σ′ tanΦ′ $_\alpha$, mobilizes first, with a negligible volume change that produces a negligible excess hydrostatic pore pressure u_e (see 12.10.3). Its ESP follows the fully drained AB. The final BC segment produces a new stable, NC state where **I** and u_e have dissipated and mobilized shear comes from only Φ′$_\beta$.

The ESP AB develops as $\mathbf{I}_\alpha$ mobilizes fully. The ESP BC develops as $\mathbf{I}_\alpha$ dissipates and one has the volume change associated with NC from σ′$_{1A}$ to 2 σ′$_{1A}$ = σ′$_{1C}$. But, from σ′$_{1A}$ to σ′$_{1B}$ one has no significant volume change and therefore no u_e to dissipate. Drainage aids would not help until σ′$_1$ > σ′$_{1B}$ or, from Equation (7), R_s exceeds the minimum (σ′$_{1B}$ /σ′$_{1A}$) and the drainage changes from only AWL viscous drainage to include primary hydrodynamic drainage.

A math study of the problem as presented in Figure 20 gives:

$$R_{S\min} = \left[\frac{(1-\tan\phi'_{\beta NC})+2\tan(\phi'_{\beta NC}+\phi'_\alpha)}{(1+\tan\phi'_{\beta NC})}\right] \quad (8)$$

A parametric study using Equation (8) produced R_{smin} in the range of 1.2 to 1.5 when using typical values of the angles involved. However, Φ′ $_{\beta NC}$ has only a minor effect and Equation (9) seems adequate.

$$R_{S\min} = 1+2\tan\phi'_\alpha \quad \text{..... (9)}$$

For the Figure 20 example, wherein Φ′ $_{\beta NC}$ = 12.8° and Φ′$_\alpha$ = 10°, R_{smin} from equation (8) equals 1.31 and from (9) equals 1.35.

Including $\mathbf{I}_c$: The above NC case neglects any $\mathbf{I}_b$ and $\mathbf{I}_c$ cohesion components. Assume any $\mathbf{I}_b$ mobilizes as part of the OCR determination in the subsequent 12.10.2.2. Further assuming the plastic and viscous $\mathbf{I}_c$ remobilizes fully from zero with the application of a surcharge, then the $\mathbf{I}_c$ cohesion would also increase R_{smin} together with the $\mathbf{I}_\alpha$ friction. The $(\sigma_1-\sigma_3)/2$ in the

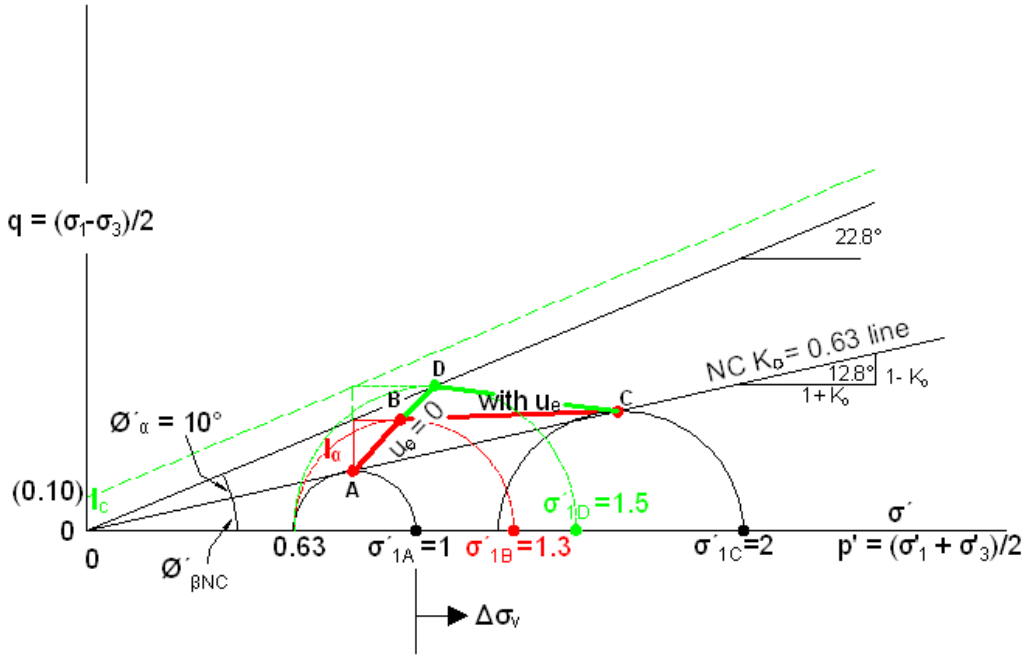

Figure 20: Effective p′-q Stress Paths for Example R_{smin}

envelope in Figure 20 would increase by a constant $\mathbf{I}_c$, as shown by the dashed line. A math study of the above increase shows that R_{smin} would increase by ($2\mathbf{I}_c/\sigma'_1$) in both equations (8) and (9). Reworking the previous example to include an $\mathbf{I}_c = 0.10$, gives R_{smin} =1.51 and 1.55, versus the previous 1.31 and 1.35. Including a range of 5 to 20 kPa for $\mathbf{I}_c$, in an example when σ'_1=100 kPa, would increase the range in R_{smin} from about 1.3 to 1.9 versus the previous 1.2 to 1.5.

12.10.2.2 Overconsolidated (OC) Case

Figure 20 can also illustrate the OC case, with NC and OC points "A" and "C" (with OCR = 2). Assume that the AC recompression occurs without significant u_e, and that a new level of **I** can mobilize at "C". The additional **I** then becomes part of the OCR and R_{smin} equals the OCR.

Hansbo and Torstensson (1977, p. 535) describe the results from research on the effectiveness of vertical drains under four test fills over soft clays. On this basis, plus wider practical experience, they emphasize and conclude that the surcharge overpressure in the clay must exceed the preconsolidation pressure. They wrote "*It is amazing how often installation of drains is considered without that those concerned knowing the preconsolidation pressure of the subsoil in question. No doubt, the non-effectiveness of vertical drains sometimes experienced can be explained by the fact that the preconsolidation pressure (p_c) is not exceeded due to loading. In such a case, the rate of consolidation is almost the same, drains or no drains, and …*"

As noted in 12.3.3, many if not most NC clays actually have a reliable p_{ca} due to ageing, with an effective OCR typically between 1.25 and 2. As shown in the previous 12.10.2.1, R_{smin} due to the mobilization of the $\mathbf{I}_\alpha$ component has a predicted range of 1.2 to 1.5, which increases to 1.3 to 1.9 when including ($\mathbf{I}_c/\sigma'_1$) = 0.05 to 0.20. It seems likely that this mobilization and subsequent AWL viscous transfer to Φ'_β could produce a p_{ca} in consolidation tests and become a part of its OCR. This might explain some of the non-effectiveness noted in the above quote when the engineers assumed NC.

12.10.3 Data and Examples

Reviewing the research data from drained NC tests on the extruded BBC, kaolinite, and Enid clays, plus 3 other clays, indicates the volume strain ϵ_v when $\mathbf{I} \approx (\mathbf{I}_c + \mathbf{I}_\alpha)$ occurs with an average $\epsilon_v \approx +0.05\%$. All the checked tests showed a small, positive dilatency. Mobilizing **I** occurs with very little volume change and with an expanding structure. It would therefore generate negligible positive pore pressure during the mobilization of ($\mathbf{I}_c + \mathbf{I}_\alpha$) when tested undrained**.** After developing the above theory and equations, the writer searched for lab and field examples to check the R_{smin} concept and found the following:

12.10.3.1 Lab

Hall (1960) provides one relevant lab example not found in Schmertmann and Hall (1961). The example shows the isotropic NC of a kaolinite to 228 kPa for 1 day, followed by an 11-step, all in one hour, drained incremental increase in (σ_1-σ_3) to 371 kPa while holding σ_3 constant at 228 kPa.

Hall found that the additional anisotropic consolidation volume change of 200 mm^3 did not begin until the additional (σ_1-σ_3) reached between 68 and 80 kPa. Hall wrote *"This would fall near the value of twice the peak cohesion (**I**) for the sample."* In this test the measured R_{smin} = [228+(68 to 80)]/228 = 1.30 to 1.35. Both $\Phi'_{\beta NC}$ and Φ'_α equaled approximately 10°, and Equations (8) and (9) would predict 1.32 and 1.35, respectively. Adding an extruded kaolinite $\mathbf{I}_c \approx 8$ kPa would increase the computed R_{smin} to 1.39 and 1.42, respectively, and still near the measured values.

Some experiments have shown that clays do not follow Darcy's Law at low gradients. They show a much lower permeability (or hydraulic conductivity) in clay when tested at low versus high gradients – for example, as suggested in Hansbo and Torstensson (1977, p. 534) and as shown in Hansbo [(1973), copied in Mitchell (1993, p. 238)]. Such behavior might occur because the low gradients move mostly the plastic-behaving and very viscous AWL water. When applying Darcy's law one must correct for permeability varying inversely proportional to viscosity. Perhaps, in a sense, there also

exists here an R_{smin} that one must exceed to begin significant "primary" laminar flow movement of low viscosity "ordinary" water. As gradients increase, perhaps one first has mostly a "secondary" slow AWL water flow followed by a mostly faster "primary" water flow, with a consequent increase in the calculated permeability during the transition.

12.10.3.2 Field

Terzaghi (1941b) presented a combination of lab and field experience that relates closely to the R_{smin} concept herein for effective wick drains. He refers to a *"critical (over) pressure, q_c"* required to break the *"solidification"* bonds formed in a layer of (NC) clay. Once broken, the clay enters the *"lubricated state"* and becomes highly compressible and *"undergoes the well known process of consolidation"*. He wrote further *"That this has been repeatedly demonstrated by direct measurement in the field"*. In the present context this means we have an $R_{smin} = (1 + q_c/\sigma'_1)$ to reach before we get the generation of u_e so that drainage aids can increase the rate of u_e dissipation.

In Terzaghi (1941b) he also wrote that *"Construction experience seems to indicate that the critical (over) pressure is of the same order of magnitude as the unconfined compression strength of the clay (q_u)."* Then:

$$R_{smin} \approx (1 + q_c/\sigma'_1) \approx (1 + q_u/\sigma'_1) \approx (1 + 2s_u/\sigma'_1) \quad ..(10)$$

Figure 20 seems to check this indication. From Figure 20, $q_u = (1\text{-}K_o)\sigma'_1 = 0.37$ and $(1+q_u/\sigma'_1) = 1.37$ using only $\mathbf{I}_\alpha$ transfer. The figure shows $R_{smin} = 1.32$. Including a typical $\mathbf{I}_c/\sigma'_1 = 0.05$ transfer increases R_{smin} to = 1.42. Thus, in this case $R_{smin} \approx (1 + q_u/\sigma'_1)$ as indicated by Terzaghi.

The above agreement may have broader implications. Long experience shows that (s_u/σ'_1) in 'NC' clays usually varies from about 0.15 to 0.40. Therefore, because $q_c \approx 2s_u$, $(1 + q_c/\sigma'_1)$ usually varies from about 1.3 to 1.8. Note the similarity to the 1.3 to 1.9 estimated range for R_{smin} developed in 12.10.2.1. Further note the typical range in **12.3** for the ageing $OCR = [(p_{ca} + p_o)/p_o] = 1.25$ to 2, based on experience. We have three similar ranges and that suggests a commonality. For example, perhaps p_{ca} increases with increasing (s_u/σ'_1)?

12.10.3.3 Practice

The writer's ageing OC, his unstable AWL $\dot{\Phi}_\alpha$ to stable $\dot{\Phi}_\beta$ (and $\mathbf{I}_b$) time-transfer to develop R_{smin}, and Terzaghi's AWL solidification and q_c may all describe the same behavior. Practically, determining p_c from high quality clay samples using a CLI oedometer test should provide a good estimate of R_{smin}. Alternatively, one can test for or otherwise estimate the **I**-components, and/or q_u or s_u and use equations (8 and 9 with an $\mathbf{I}_c/\sigma'_1$ addition) and/or (10) to estimate R_{smin}.

12.11 Failure Planes and Slickensides

The one and two specimen **IDS**-test comparisons in Schmertmann (1962), while good enough to show the utility of curve hopping (see **3.2**), do show a general tendency for $\dot{\Phi}_\alpha$ to decrease and $\dot{\Phi}_\beta$ to increase with $\dot{\epsilon}$ in the two specimen versus one specimen tests. This provides still another example of the Φ'_α to Φ'_β time transfer behavior over the approximate 10 hour time of a typical constant $\dot{\epsilon}$ test. The curve hopping in the one specimen test disrupts and slows the transfer compared to the matching two specimen test without the hopping.

Strain disrupts and changes a clay's structure. Strain and time make it progressively easier for the AWL $\dot{\Phi}_\alpha$ secondary shear reduction to increase the Φ'_β primary shear.

Disrupting structure to the point of developing a visible failure plane concentrates and increases the shear strain on that plane. This tends to deflocculate and disperse the clay's structure into a more parallel arrangement of its platy particles in the direction of the failure plane. This in turn appears to make it easier for the AWL to attract water to the particles. Whatever the reason, the apparent viscosity of the AWL reduces, Φ'_α decreases, and therefore more easily transfers to Φ'_β. Schmertmann and Osterberg (1960, Fig. 13), and Schmertmann (1976, Fig 5 and 1981, Fig 2) show one of many examples of the accelerated $\dot{\Phi}_\alpha$ to Φ'_β (**I** to **D**) transfer resulting from a failure plane.

The failure plane eventually becomes a slickenside with ageing and insitu movements along that plane. Its parallel fabric minimizes opportunities for stable particle/particle interference and bonding, but maximizes the surfaces for unstable AWL lubrication. We thus have a preferential surface for shear movement and creep. With enough of this minimizing and maximizing the clay approaches the residual state, controlled primarily by the AWL as suggested in **12.1**.

12.12 Creep and the I-component in Drained Compression

As discussed previously, the viscous behavior of the AWL reduces the stability of a clay's structure and causes the time-transfer of mobilized shear to the more stable bond and particle interference components $\mathbf{I}_b$ and Φ'_β, respectively. The transfer also produces creep. The writer will now present experimental evidence to show that the mobilization of the unstable $\mathbf{I}_c$ and $\mathbf{I}_\alpha$ components do not initially produce significant creep until they mobilize fully. The discussion in **12.11** already suggested that **I** must mobilize fully before significant destructuring can occur to generate u_e excess pore pressure. The same appears true for creep in kaolinite clay, as shown below, and perhaps in many other clays. But, as discussed in **12.1** once creep has begun Φ'_α may transfer to Φ'_β and remobilize in cycles that depend on the loading cycles.

12.12.1 Creep Limit

There exists a convenient test and graphical method for obtaining the pressure or stress limit at which significant creep will begin in clay. The test involves incremental load increases and stress control to permit creep at constant stress. As shown in the subsequently discussed Figure 21 example, the writer plotted a creep strain increment ($\Delta\epsilon$) versus the constant $\sigma_a = (\sigma_1 - \sigma_3)$ for that increment. Such plots often produce bi-linear and/or tri-linear slopes. Their intersections define "creep limits" (CL_1 and CL_2 in Figure 21) useful in practice to predict the loading at which significant creep and failure will begin. Housel (1959) showed the use of this method for avoiding creep movement problems in Detroit clays. Stoll (1961) used the method to demonstrate that the creep limit CL_1 applied to piles in both sand and clay. The ASTM Pressuremeter Standard D4719 includes a similar method to determine a creep limit CL_1 from pressuremeter testing. Loadtest Inc. has used the method routinely for pile side shear and end bearing creep limit estimates for over 11 years and most of their pile test reports include an appendix describing it. The method works best with constant increments of loading and a fixed time interval for the determination of creep strains.

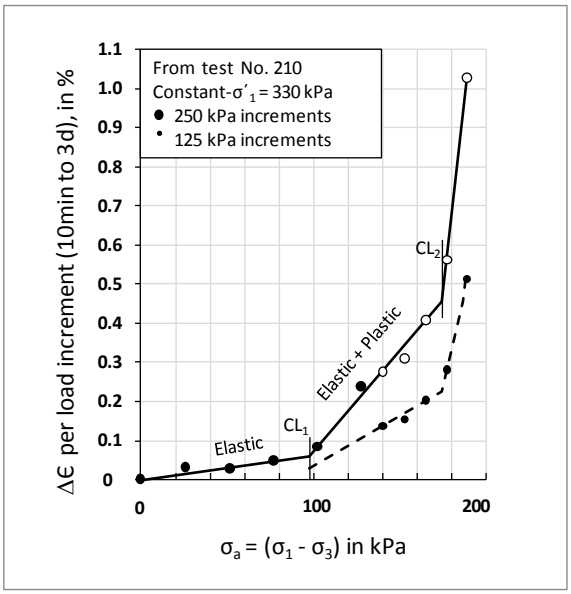

Figure 21: Constant Dead Load, Drained Compression, Creep Limits in Kaolinite

12.12.2 Test Examples

Section **8.1** describes the results from Bea's (1960) undrained creep and **IDS**-testing using extruded kaolinite and extruded and 'undisturbed' BBC. These tests all showed a time transfer from the **I** to the **D** component during creep. They all had a final creep strain that exceeded the strain to reach $\mathbf{I}_{max}$.

Now consider some drained creep data from the stress-controlled, constant–σ'_1, compression tests similar to those in Figure 9(a). First we consolidated isotropically for one day to $\sigma'_c = 350$kPa and rebounded to a reduced σ'_1 of 330 (tests 210, 219) or 260 kPa. We then held each axial load increment constant for approximately three days, and measured the creep strain for each over the 10min to 3day

time interval after applying each increment. Matching increments of σ_a by imposing an equal increment of pore pressure kept σ'_1 constant and reduced σ'_3. Figure 21 shows the creep graph for the constant–σ'_1 = 330kPa test No. 210. For this test we applied 5 initial increments of $\Delta\sigma_a$ = 250kPa followed by 5 increments of $\Delta\sigma_a$ = 125kPa. The writer then doubled the 125kPa increment creep to permit comparing with the prior 250kPa increment data. This doubling seemed logical and appeared to produce consistent results. Figure 21 shows both sets of points.

The plotted data from test No.210 show two linear slope intersections, CL_1 at σ_a = 97kPa and CL_2 at σ_a = 174kPa. The matching ϵ values ≈ 0.2% and 1.1%. Similar to the interpretation used for pressuremeter tests, the writer has labeled the resulting 0 to CL_1 slope as "elastic", CL_1 to CL_2 as "elastic + plastic", and greater than CL_2 as "plastic to failure". As discussed subsequently, the writer performed 3 more tests similar to No.210 and all produced similar CL_1 and CL_2 results.

Note that only small volume changes occurred during these 4 drained creep tests because of using constant–σ'_1 values below σ'_c. The specimens actually expanded, or swelled slightly because of the progressive reduction of σ'_3 with σ_a. The writer assumed that this swelling had a negligible effect on $\Delta\epsilon$ creep and the limit interpretations in Figure 21.

12.12.3 $CL_1 \approx 2\ I_{max}$

As developed in this paper, viscous plastic behavior results from the cohesive and frictional shear components that mobilize as particles slide along their AWL contacts. This sliding produces creep. Assuming negligible bonding in the machine extruded specimens used for the Figure 9 tests, the creep should occur in conjunction with the AWL **I** to Φ'_β component transfer behavior. Figure 9(b) shows that it does.

At the CL_1 strain of 0.2% in duplicate test No. 210 in Figure 21, **I** in test 219 in Figure 9(b) has reached an $\mathbf{I}_{max}$ shear of 50 kPa with an approximate compressive strength mobilization of 2 $\mathbf{I}_{max}$ = 100kPa. Thus, the above CL_1 = 97kPa closely matches that expected from only the **I** component. All the stress controlled tests in this 4-test creep study produced similar CL_1 values of 97 to 100kPa.

12.12.4 Elastic I_{max}

Section 12.10.3 has already discussed lab anisotropic consolidation and field surcharge test results as part of the discussion of Figure 20. The results indicate a $u_e \approx 0$, low volume change, pseudo-elastic behavior during the mobilization of the **I** component of shear. The previous 12.12.3 also suggests an elastic mobilization of $\mathbf{I}_{max}$ before starting significant compressive creep.

The destructuring or yielding of a clay during creep occurs in association with the viscous transfer from the unstable AWL components, $\mathbf{I}_c$ and $\mathbf{I}_\alpha$, to the stable $\mathbf{I}_b$ and Φ'_β components. The lack of significant creep from σ_a = 0 to $\mathbf{I}_{max}$ may also indicate the lack of significant transfer until after **I** mobilizes to $\mathbf{I}_{max}$. Many (Figs. 4, 5, 9, 11, 12, 13) of the 2-specimen, strain controlled, **IDS**-tests in Schmertmann (1962) show a very similar **I** and Φ'_β (then called c_ϵ and Φ_ϵ) versus strain behavior when compared to the results presented in Figure 9. After $\mathbf{I}_{max}$, and with continuing strain, one again sees a noticeable transfer from **I** to Φ'_β. In hindsight these 1962 tests already showed that the transfer may occur only after **I** reaches $\mathbf{I}_{max}$ and thus further support the concept of its pseudo-elastic mobilization.

12.12.5 (CL_1/CL_2) Creep Ratio

Prandtl's solution for the plane strain, bearing capacity problem on a weightless, frictionless soil, and which assumes ideal [(elastic + (elastic + plastic)] shear behavior, gives the ratio of [(elastic loading to the beginning of plastic shear along the failure surface)/(failure by plastic shear along the entire surface)] = [$\pi/(\pi+2)$] = 0.61. The same ratio from test No. 210 in Figure 21, (CL_1/CL_2) = (97kPa/174kPa) = 0.56, and (100/156) = 0.64 in a duplicate test No. 219 (not shown). The two tests averaged 0.60 versus the theoretical 0.61.

The above close agreement between elastic-plastic bearing theory and creep behavior supports the concept that CL_1 indicates a transition from elastic deformation to (elastic + plastic)

creep, and that CL_2 indicates the transition to a fully plastic creep failure in kaolinite clay.

Tests 210 and 219 had an isotropic (σ'_C/σ'_1) = OCR = (350kPa/330kPa) = 1.06. Two additional very similar tests, but with constant σ'_1 = 260kPa and an OCR of 1.35, both had $(CL_1/CL_2) \approx 0.73$. The above 0.60 versus 0.73 suggests that (CL_1/CL_2) increases with OCR and therefore this kaolinite clay behaved more elastically with increasing OCR and follows this general experience with almost all clays.

12.13 Drained and Undrained Shear Components

Laboratory research and field design methods for clay often differentiate between two ideal extreme drainage conditions—completely drained or undrained. In saturated soils the former permits volume change but no significant excess pore pressure, u_e, and the latter permits no significant volume change and the development of u_e. One can easily model these extremes in the laboratory by simply turning a drainage valve between open and closed. In the field the drainage always occurs somewhere between the extremes. However, for **IDS**-testing and shear component determinations the presence or absence of u_e does not matter. As shown below, only effective stress matters.

No back Pressure Effect: Numerous **IDS**-tests with and without back pressure of various magnitudes, but with the same effective stresses, showed no difference in the shear components and their mobilization with strain.

Same Drained and Undrained Test Results: The drained tests discussed herein in detail involved controlling pore pressure to match σ_a and thereby keeping σ'_1 constant. They produced the narrow range in Φ'_α and $\mathbf{I}_c$ values shown in Figures 13 and 15 and in Schmertmann (1976, Fig. 12). Undrained tests, as shown in Schmertmann (1976, Figs. 17, 18, 19), produce similar Φ'_α and $\mathbf{I}_c$ values.

With undrained tests one curve hops between two values of constant volume, measures u_e, and analyzes the results in terms of effective stress using the same method as in Figure 1. However, the undrained tests may have less accuracy in the component separations because one can usually measure an independently imposed pore pressure more accurately than the u_e developed in response to stress and strain in an undrained test.

Same Φ'_α to Φ'_β Creep Transfer: Section **8.1** and the associated references described some undrained, stress controlled, creep and **IDS**-test experiments by Bea. They showed a transfer from Φ'_α to Φ'_β during undrained creep. Section **12.12** just demonstrated and discussed the same transfer during drained creep. Qualitatively, both show the same time-transfer in the Φ'_α to Φ'_β friction components. However, the strain rate and magnitude of transfer may, or may not, differ significantly because effective stresses change more rapidly in undrained tests due to the uncontrolled u_e.

13. SUMMARY COMMENTS AND CONCLUSIONS

This research focused on determining the more fundamental engineering components of shear resistance in clays and their relation to strain, structure and time. The writer used the simplest suitable tools and model available at the time, namely the M-C model and the axisymmetric triaxial test. The following results, as developed herein, support this simple approach and should provide a significant step forward in understanding the engineering shear behavior of clay.

13.1 As explained and demonstrated herein, the **IDS**-test provides data for the more fundamental evaluation of the Mohr-Coulomb shear components of soils, including clays. Its use also permits investigating **the important effects of strain, strain-rate and time**.

13.2 A strain-controlled, **IDS**-test on a single specimen of extruded clay mobilizes two distinct groups of components of shear resistance, namely **I** and **D**.

13.3 All test comparisons show that the $\mathbf{I}_\alpha$ part of the **I** 'nominal cohesion' component varies linearly with effective stress. $\mathbf{I}_\alpha$ therefore does not behave as a cohesion but **instead behaves as an engineering friction**, denoted Φ'_α with $\mathbf{I}_\alpha = \sigma' \tan \Phi'_\alpha$. This Φ'_α presents an apparent paradox, compounded by its insensitivity to interlocking, void ratio and OC, plus its transient and plastic behavior, all of which the writer explains by the behavior of

the adsorbed water layer (AWL). Additional data relating Φ'_{α} to grain size, $\Phi'_{residual}$, secondary consolidation, creep, G_o, and p_{ca} provide additional support for this explanation.

13.4 The results from this study support the concept of two dominant clay friction components – a "secondary", viscous Φ'_{α} due to lubricated sliding in the adsorbed water layers, and a "primary" stable Φ'_{β} due to particle geometrical interference effects. The two frictions behave very differently with respect to interlocking and dilatency, and stress, strain and time paths.

13.5 Linear Mohr envelope extrapolations to the origin determine the intercept $\mathbf{I}_c$ when constructing the envelope at constant strain. $\mathbf{I}_c$ measures a real cohesion in extruded (severely remolded) clays, as confirmed by triaxial effective stress tension and stress-dilatency tests of the kaolinite. $\mathbf{I} = \mathbf{I}_c + \mathbf{I}_{\alpha}$ and therefore includes both engineering cohesion and friction.

13.6 $\mathbf{I}_c$ behaves plastically when $\epsilon \geq 0.5\%$ and therefore also seems to result from viscous AWL behavior.

13.7 Overconsolidation does not produce a significant change in the **I**-component at a given effective stress and strain. It does increase the **D**-component [σ' tan $\Phi'' \approx \Phi'_{\beta}$)] and **D** mobilizes earlier with strain as the OCR increases. OC, at a given strain, increases the "primary" Φ'_{β} but not the "secondary" Φ'_{α}.

13.8 The writer found important component time effects in both the shear and the related consolidation behavior of clays. He believes these effects result from the viscous-transient shear behavior of the particle boundary adsorbed water layer and from the more brittle cohesive bonds that can form with time.

13.9 Important differences in the measured values of the components can occur as a result of stress control testing with rest times versus the often more convenient constant strain rate control testing. The component time transfer effects may not occur during strain control or they may occur much more slowly.

13.10 Creep at strains less than residual can produce an important increase in the Φ'_{β} capability of a clay. The soil structure changes that accompany creep also produce an increase in the shear resistance of a clay mobilized at the same strain after creep versus without the creep. This can occur in both drained and undrained creep provided the clay structure and/or time available permits Φ'_{β} to increase.

13.11 If Φ'_{β} can increase, stress-controlled creep with time intervals of rest can provide a reserve strength increase of at least 10% at the same additional strain in the tests described herein. For the creep associated with K_o anisotropic normal consolidation, this increase may = 50% or more.

13.12 The more stable clay friction component that does not appear to have transient decay in this research, Φ'', which $\approx \Phi'_{\beta}$, seems to result from particle geometrical interference effects as shown, at a given **IDS**-test strain, by its increase with reduced void ratio, drained and undrained creep, OC and interlocking, and (from references) a more deflocculated/dispersed structure.

13.13 The formation of bonds can inhibit the low strain mobilization of the particle interference Φ'_{β}.

13.14 The **I**-component appears to behave elastically and may require full mobilization before the Φ'_{α} to Φ'_{β} clay structure's stability transfer and plastic creep begin.

13.15 The shear components and their mobilization depend on effective stress and time, and not on whether one tests the specimen drained or undrained.

13.16 The thirteen practical concepts discussed herein show how component behavior can help to explain the causes of residual shear, secondary consolidation, secondary shear, ageing preconsolidation, an applicability to silts, sands, and partially saturated soils, undrained strength insensitive to effective stress, very viscous AWL behavior in the small strain shear modulus, the use of Φ'_{β} when determining K_o, different types of consolidation, Burland's ICL, the minimum surcharge ratio for effective drainage aids, failure planes and slickensides, creep, and the similarity between the drained and undrained shear components.

14. ACKNOWLEDGEMENTS

The writer received important encouragement to pursue his shear strength investigations from Drs.

Jorj Osterberg, Frank Richart Jr. and Karl Terzaghi, but especially from Laurits Bjerrum, the first Director of the Norwegian Geotechnical Institute. Dr. Bjerrum arranged with Arild Andresen of Geonor Inc. for the University of Florida to purchase the high quality triaxial test equipment that made the research possible, provided the opportunity for a 1962-3 postdoctoral fellowship at the NGI, as well as guidance by personal conversations and correspondence. Many students contributed by their research, including Robert Bea, John Hall Jr., KumHung Ho, Helle Strømann and Anne Topshøj. William Whitehead contributed important engineering technician support. Financial support came from three research grants and a post-doctoral fellowship from The National Science Foundation, all supplemented generously by the University of Florida Engineering Experiment Station. Neil Schmertmann helped prepare large spreadsheets of **IDS**-test data and performed the analyses involved to prepare Figures 2, 3 and 5. Michael Ahrens of Loadtest, Inc. also helped with these figures. Suzanne Turner, also from Loadtest, Inc., provided word processing and figure preparation assistance.

15. REFERENCES

Anderson, D. G. and F. E. Richart, Jr. 1974, "Temperature Effect on Shear Wave Velocity in Clays", Technical Note, ASCE Journal of Geotechnical Engineering Division, V100, GT12, pp. 1316-1320. Also in ASCE, GSP 1, p. 16 and GSP 118, p. 1603.

Anderson, D. G. and R. D. Woods 1976, "Time-Dependent Increase in Shear Modulus of Clay", ASCE Journal of the Geotechnical Engineering Division, V102, GT5, May, pp. 525-537.

Bea, R. G. 1960, An experimental study of cohesion and friction during creep in saturated clay. Master's thesis to the University of Florida, 107 pp., published in part by Bea (1963).

Bea, R. G. 1963, Discussion on: Wu, T. H., A. G. Douglas and R. D. Goughmour: Friction and cohesion of saturated clays. A summary of Bea 1960. American Society of Civil Engineers, Journal of the Soil Mechanics and Foundations Division, Vol. 89, No. SM1, pp. 268-277.

Bishop, A. W. and V. K. Garga 1969, "Drained tension tests on London clay", Geotechnique, Vol. XIX, No. 2, pp. 309-313.

Bjerrum, L. 1967a, "Engineering geology of Norwegian normally consolidated clays as related to settlements of buildings", Geotechnique, Vol. 17, pp. 81-118. The 7th Rankine Lecture, reprinted in NGI Publication Nr. 71.

Bjerrum, L. 1967b, "Progressive Failure in Slopes of Overconsolidated Plastic Clay and Clay Shales", The 3rd Terzaghi Lecture, ASCE, JSMFD V93, Part 1, p.16

Bjerrum, L. 1972, "Embankments on Soft Ground", ASCE Proceedings of the Specialty Conference on PERFORMANCE OF EARTH AND EARTH-SUPPORTED STRUCTURES, Vol. II, p. 20.

Bjerrum, L. 1973, "Problems of soil mechanics and construction on soft clays.", State-of-the-art- Paper to Session IV, 8th ICSM & FE, Moscow, Vol. 3, pp. 124, 134.

Burland, J. B., 1990, "On the compressibility and shear strength of natural clays", Geotechnique, V40, 329.

Burland, J.B., Jamiolkowski, M.B., and Viggiani, C. 2009, "Leaning Tower of Pisa: Behavior after Stabilisation Works", Final Draft, to be published in the International Journal of Geoengineering Case Histories.

Casagrande, A. 1932, "The Structure of Clay and its Importance in Foundation Engineering", Journal of the Boston Society of Civil Engineers, April. Reprinted in BSCE Contributions to Soil Mechanics 1925-1940, pp. 72-125.

Casagrande, A. 1950, "Notes on the Design of Earth Dams", Journal of the Boston Society of Civil Engineers, Vol. XXXVII, October. Reprinted in BSCE Contributions to Soil Mechanics 1941-1953, pp. 231-255.

Crawford, C. B. and Burn, K. N. 1976, "Long-term settlements on sensitive clay", Laurits Bjerrum Memorial Volume, NGI, pp. 117-124.

Duncan, J. M. 1991, "The Importance of a Desiccated Crust on Clay Settlements", Soils and Foundations, Vol. 31, No., 3, p. 83.

Ellstein, A. 1992, Discussion of Schmertmann 1991, Journal of Geotechnical Engineering, ASCE, Vol. 118, No. 12, Dec., p. 2012.

Failmezger, R. and Bullock, P. 2008 "Which in-situ test should I use? - A designer's guide", paper submitted for publication by ASCE in Proceedings of Foundations Expo '09, Orlando

Hall, J. Jr. 1960, "An Experimental Study of the Effect of Anisotropical Consolidation on the Cohesion and Friction in Saturated Clay", Master of Science Thesis, University of Florida, p. 29

Hamel 2004, discussion of Mesri et. al., ASCE JGGE, May, p.545

Hansbo, S. 1973, "Influence of mobile particles in soft clay on permeability", Proceedings of the International Symposium of Soil Structure, Gothenburg, Sweden, pp. 132-135.

Hansbo, S. and Torstensson, B. A. 1977, "Geodrain and other Vertical Drain Behavior", Proceedings of the 10th ICSMFE, Tokyo, V.2., p.535.

Ho, K-H 1971, "Theoretical and Experimental Relationships between Stress Dilatancy and IDS Strength Components", University of Florida, Dept. of Civil Engineering, PhD dissertation, 230 pp., unpublished

Horn, H. M., and Deere, D. U. 1962, "Frictional characteristics of minerals", Geotechnique, Vol. 12, No. 4, pp. 319-335.

Horslev, M. J. 1961, "Physical Components of the Shear Strength of Saturated Clays", American Society of Civil Engineers Research Conference on Shear Strength of Cohesive Soils, p. 169.

Housel, W. S. 1959, "Dynamic & Static Resistance of Cohesive Soils", ASTM STP 254, pp. 22-23

Hutchinson, J.N. 1967, "The Free Degradation of London Clay Cliffs", Proceedings of the Geotechnical Conference Oslo 1967 – on Shear Strength Properties

of Natural Soils and Rocks, V.I, p.118

Kenney, T.C. 1967a, "The Influence of Mineral Composition on the Residual Strength of Natural Soils", Proceedings of the Geotechnical Conference Oslo 1967 – on Shear Strength Properties of Natural Soils and Rocks, V.I, p.129

Kenney, T.C. 1967b, "The Influence of Mineral Composition on the Residual Strength of Natural Soils", Proceedings of the Geotechnical Conference Oslo 1967 – on Shear Strength Properties of Natural Soils and Rocks, V.I, p.50

Lacasse, S., Berre, T. and Lefebvre, G. 1985, "Block sampling of sensitive clays", Proc 11th Int. Conf. on Soil Mech., San Francisco, 2, 887-892.

Lambe, T. W. 1953, "The Structure of Inorganic Soil", American Society of Civil Engineers, Proceedings, Vol. 79, Separate No. 315.

Lambe, T. W. 1958, "The Structure of Compacted Clay", ASCE Journal Soil Mechanics and Foundation Division, V. 84, No. SM2, May.

Lambe, T. W. 1960, "A Mechanistic Picture of Shear Strength in Clay", Proceedings Research Conference on Shear Strength of Cohesive Soils, ASCE, Boulder, Colo., pp. 555-580.

Landva, A., Valsangkar, A. J. and Alkins, J. C. 1988, "Performance of a Raft Foundation Supporting a Multistory Structure", Canadian Geotechnical Journal, Feb., see Figure 2, p. 140.

Landva, A. 2006, "A closer look at K_o=sin Φ' " 59th Canadian Geotechnical Conference, Oct 1-4, Vancouver, BC, pp.291-296.

Larsson, R. 1986, "Consolidation of soft soils", Swedish Geotechnical Institute, Report No. 29, p. 81.

Leonards, G. A. 1972 discussion, ASCE, Performance of Earth and Earth-Supported Structures, Purdue Univ., VIII, p.169.

Leroueil, S. 1996, "Compressibility of Clays: Fundamental and Practical Aspects", ASCE JGE, V122, N7, July, pp. 535, 541. Also in ASCE, GSP No. 40, pp. 63-65.

Low, H-E, Phoon, K-K, Tan, T-S, Leroueil, S 2008, "Effect of soil microstructure on the compressibility of natural Singapore marine clay", Can. Geotech. J. 45, pp. 161-176

Lunne, T., T. Berre and S. Strandvik 1997, "Sample disturbance effects in soft low plastic Norwegian clay", Proceedings of the International Symposium on Recent Developments in Soil and Pavement Mechanics, Rio de Janeiro, Brazil, A. A. Balkema, Rotterdam, pp. 81-102.

Matlock, H., C. W. Fenske and R. F. Dawson 1951: "De-aired, extruded soil specimens for research and for evaluation of test procedures", American Society for Testing and Materials, Bulletin 177, October pp. 51-55.

Mayne, P.W. and Kulhawy, F.H. 1982 "K_o – OCR Relationship in Soil" J. Geotech. Eng. Div., ASCE, 108(6), 851-872.

Mesri, G., Feng, T. W., and J. M. Benak 1990, "Post-densification Penetration Resistance of Clean Sands", ASCE Journal of Geotechnical Engineering, V116, No. 7, pp. 1095-1115.

Mitchell, J. K. 1976, Fundamentals of Soil Behavior, John Wiley & Sons, Inc..

Mitchell, J. K. 1993, Fundamentals of Soil Behavior, 2nd Ed., John Wiley & Sons, Inc., pp. 366, 370.

Mitchell, J. K. 2008, "Aging of Sand – A Continuing Enigma?", 6th Intl. Conference on Case Histories in Geotechnical Engineering, Arlington, VA Aug 11-16, 2008, Paper No.SOAP 11

Morgenstern, N. R. 1967, "Shear Strength of Stiff Clays", Proceedings of the Geotechnical Conference Oslo 1967 – on Shear Strength Properties of Natural Soils and Rocks, V.I, p.67

Perkins, S. W., and M. Sjursen 2009, "Effect of cold temperatures on properties of unfrozen Troll clay", Canadian Geotechnical Journal, NOTE, V46, N12, pp. 1473-1481.

Rowe, P. W. 1957: "c_e = 0 hypothesis for normally loaded clays at equilibrium", 4th I.C.S.M. & F. E., London, Vol. 1, p. 189.

Rowe, P. W. 1962: "The stress-dilatancy relation for static equilibrium of an assembly of particles in contact", Proceedings of the Royal Society, A, Vol. 269, pp. 500-527.

Rowe, P. W., Oates, D. B. and Skermer, N. A. 1963, "The Stress-Dilatancy Performance of Two Clays", ASTM Special Publication No. 361, pp. 134-146.

Rowe, P.W.; Barden, L. and Lee, I. K. 1964 "Energy Component During the Triaxial Cell and Direct Shear Tests", Geotechnique, Vol. 14, pp. 247-261.

Schmertmann, J. H. 1962, "Comparison of one and two-specimen CFS (**IDS**) tests. American Society of Civil Engineers, Journal of the Soil Mechanics and Foundation Division, Vol. 88, No. SM6, pp. 169-205.

Schmertmann, J. H. 1963, Discussion on O'Neil, H. M., Direct-shear test for effective strength parameters. American Society of Civil Engineers, Journal of the Soil Mechanics and Foundations Division, Vol. 89, No. SM3, Part 1, pp. 159-161.

Schmertmann, J. H. 1964 "Generalizing and Measuring the Hvorslev Components of Shear in Clays", ASTM STP 351, pp. 147-162. Reprinted in ASCE GeoInstitute *GSP-180,* FROM RESEARCH TO PRACTICE in GeotechnIcal Engineering honoring J. H. Schmertmann, pp. 34-44.

Schmertmann, J. H. 1976 "The Shear Behavior of Soil with Constant Structure", Laurits Bjerrum Memorial Volume, Norwegian Geotechnical Institute, Oslo, pp. 65-98.

Schmertmann, J. H. 1981, "A General Time-Related Soil Friction Increase Phenomenon", ASTM Special Technical Publication No. 740, pp. 456-484.

Schmertmann, J. H. 1983, "A Simple Question About Consolidation", ASCE Journal of Geotechnical Engineering, Technical Note, Vol. 109, No. 1, pp. 119-122. Discussions and Closure in Vol. 110, No. 5, May 1984, pp. 665-673.

Schmertmann, J. H. 1991, "Mechanical Aging of Soils (25th Terzaghi Lecture)". Journal of Geotechnical Engineering, Vol. 117, No. 9, see pp. 1308-1325.

Schmertmann, J. H. 1993, "Update on the Mechanical Aging of Soils (25th Terzaghi Lecture)", Symposium, titled "Sobre Envejecimiento de Suelos", sponsored by The Mexican Society of Soil Mechanics, Mexico City, 26 Aug 93.

Schmertmann, J. H. 2003, Discussion of "Yielding from Field Behavior and its Influence on Oil Tank Settlements" by Riccardo Berardi and Renato Lancellotta, JGGE, Vol. 129, No. 5, p. 481.

Schmertmann, J. H. and Hall, J. R. Jr. 1961: "Cohesion after non-isotropic consolidation", American Society of Civil Engineers, Transactions, Vol. 128, Part I, pp. 949-981. Also publ. in A.S.C.E. as Proceedings Paper 2881, Journal of the Soil Mechanics and Foundation Division, Aug., 1961.

Schmertmann, J. H. and Osterberg, J. O. 1960. "An experimental study of the development of cohesion and friction with axial strain in saturated cohesive soils", Proceedings Research Conference on Shear Strength of Cohesive Soils, ASCE, Boulder, Colo., 643-694

Schofield, A., 1999, "A Note on Taylor's Interlocking and Terzaghi's "True Cohesion" Error", Geotechnical News, V. 17, N4, December

Schofield, A., 2005, "Interlocking, and Peak and Design Strengths", Geotechnique, Letter to the Editor, Vol. 56, No. 5, pp. 357-358.

Schofield, A. and Wroth, P. 1968, Critical state soil mechanics, McGraw-Hill Book Company, 310pp.

Skempton, A.W. 1953, "The colloidal 'activity' of clays", Proc. 3rd Int. Conf. Soil Mechanics, Zurich, V. 1, pp. 57-61. Reprinted in Selected Papers on Soil Mechanics by A. W. Skempton, F.R.S., Tomas Telford Ltd., London, 1984.

Skempton, A.W. 1961, "Effective Stress in soils, Concrete and Rocks", in Pore pressure and suction in soils, Butterworths, London, pp. 4-16. Reprinted in Selected Papers on Soil Mechanics by A.W. Skempton, F.R.S., Thomas Telford Ltd., London, 1984, pp. 106-118.

Skempton, A. W. 1970, "The consolidation of clays by gravitational compaction", Q. J. Geol. Soc. Lond., V 125, pp. 373-412. Reprinted in Selected Papers on Soil Mechanics by A. W.

Smith, R.E., Jahangir, M.E., Rinker, W.C., 2006, "Selection of Design Strengths for Overconsolidated Clays and Clay Shales", 40th Symposium on Engineering Geology and Geotechnica Engineering, Utah State University, Logan, UT, May 24-26.

Soydemir, C. 1984, (Discussion, see Schmertmann, 1983)

Stoll, M.U.W. 1961, Discussion, Proc. 5th ICSMFE, Paris, Vol. III, pp. 279-281

Strømann, H. 1971, "Laboratory Test Techniques for Determining the Constant-Structure Envelopes of Soils", MSCE Thesis, University of Florida, 136 pp., unpublished.

Taylor, D.W. 1942, "Research on consolidation of clays" Serial 82, Massachusetts Inst. of Technol., Cambridge, Mass., 147 pp.

Taylor, D.W. 1948, Fundamentals of Soil Mechanics, John Wiley & Sons, 700 pp.

Terzaghi, K. 1920, "New Facts About Surface Friction", The Physical Review, N.S., Vol. XVI, No. 1, July. Reprinted in From Theory to Practice in Soil Mechanics, Selections of the writing of Karl Terzaghi, 1960, John Wiley & Sons, p. 165.

Terzaghi, K. 1931, "The Static Rigidity of Clays", Journal of Rheology, Vol. 2, No. 3

Terzaghi, K. 1941a. "Undisturbed Clay Samples and Undisturbed Clays". Journal of the Boston Society of Civil Engineers, Vol. xxvii, July. Reprinted in BSCE Contributions to Soil Mechanics 1941-1953, pp. 45-65.

Terzaghi, K. 1941b, "Settlement of Pile Foundations due to Secondary Compression," Proceedings of the Fourth Texas Conference on Soil Mechanics and Foundation Engineering, The University of Texas, Austin, 6pp.

Terzaghi, K. 1943, Theoretical Soil Mechanics, 5th Ed., John Wiley & Sons, p. 181.

Terzaghi, K. 1955, "Influence of Geological Factors on the Engineering Properties of Sediments", Harvard Soil Mechanics Series No. 50, Reprinted from ECONOMIC GEOLOGY 15th Anniversary Volume pp. 557-618

Terzaghi, K., Peck, R.B. and Mesri, G. 1996, Soil Mechanics in Engineering Practice, 3rd Ed., John Wiley & Sons, p. 147.

Tiwari, B., Brandon, T.L., Hideaki, M., and Gyanu R.T. 2005, "Comparison of Residual Shear Strengths from Back Analysis and Ring Shear Tests on Undisturbed and Remolded Specimens", ASCE JGGE, September, p. 1071

Topshøj, A. G. 1970, "Bond strength of extruded Kaolinite by triaxial extension testing", MSCE Thesis, University of Florida, 84 pp., unpublished.

16. NOTATION

The writer usually explains symbols and other notation when they first appear. This paper uses kPa for all stresses, as transferred from original kg/cm^2 units by taking 1 kg/cm^2 = 100 kPa. Thus, this paper has a uniform +2% error in the stresses reported herein, which the writer assumed negligible for the purposes of the paper.

A = total shear plane area per contact a
AWL = adsorbed water layer (also double layer, boundary water layer, etc.)
a = contact area of adsorbed layers between particles wherein the layers do not transmit pore pressures
BBC = Boston blue clay
C = Centigrade
C_c = "primary" consolidation $\Delta e/\Delta \log \sigma'$
C_α = "secondary" consolidation $\Delta e/\Delta \log t$
c′ = cohesion intercept from the τ_t versus σ'_t Mohr envelope
c'_{res} = c′ from non-**IDS** residual shear tests
CLI = Constant Load Increment
CRS = Constant Rate of Strain
CSME = Constant Structure Mohr Envelope developed in Schmertmann (1976, pp.65,76)
CSSM = Critical State Soil Mechanics
D = slope component from an **IDS**-test
d = days
d_{10} = particle size with 10% smaller particles, by weight
E = Young's modulus in axial compression
e = void ratio
e_i = Initial e of specimen
e_f = final e of specimen

e_{LL} = void ratio at liquid limit
G = shear modulus
G_o = dynamic low strain shear modulus
h = hours
IDS-test = triaxial test (in this paper) that determines the **I** and **D** components as functions of **S**tructure and **S**train. Called the CFS-test before 1964.
I = Intercept component from an **IDS**-test when σ′ = 0, extrapolated
$\mathbf{I}_b$ = part of **I** due to relatively brittle, non-viscous bonds
$\mathbf{I}_c$ = part of **I** due to plastic cohesion
$\mathbf{I}_m$ = maximum value of **I** in an **IDS**-test (Fig. 1d)
$\mathbf{I}_o$ = shear at σ′ = 0 from Topshøj's (1970) tension tests, or from Strømann's (1971) relaxation tests
$\mathbf{I}_t$ = **I** on plane of "t"
$\mathbf{I}_\alpha$ = part of **I** due to $\Phi'_\alpha = \sigma' \tan \Phi'_\alpha$
ICL = intrinsic consolidation line
JSC = Jacksonville sandy clay
K = $(\sigma'_{3c}/\sigma'_{1c})$
K_o = K during one dimensional consolidation
kPa = kiloPascals
k_v = coefficient of permeability (hydraulic conductivity) in vertical direction
LWC = Lake Wauburg Clay
M-C = Mohr-Coulomb
min = minutes
NC = normally consolidated
NGI = Norwegian Geotechnical Institute
OC = overconsolidated
OCR = overconsolidation ratio = σ'_c/σ'_{cu}, not including additional OC due to reduced σ'_1 during an **IDS**-test.
p = normal consolidation pressure
p_0 = p due to overburden
p_c = preconsolidation pressure
p_{ca} = additional p_c due to ageing
PI = plasticity index (%)
q_c = Terzaghi's (1941b) critical pressure
q_u = unconfined compressive strength
R^2 = a statistical measure of the accuracy of a curve fit through data
R_s = surcharge ratio (eqn. 7)
R_{smin} = minimum R_s for effective drains
S = Clay structure, including changes due to strain
S_a = the shear force transmitted per contact area a
s_u = undrained shear strength
t = point of tangency in an **IDS**-test (Fig. 1c), time
t_{100} = isotropic consolidation time for ≈ 100% primary effective stress increase
U = 'undisturbed' specimen
u = pore pressure
u_e = excess hydrostatic pore pressure
w = water content (%)
Δ = change in a value
Є = axial strain (+ compression)
$\dot{\text{Є}}$ = time rate of Є
Φ = friction angle
Φ′ = Φ from the effective stress Mohr envelope used herein and mobilized at constant Є with $\dot{\text{Є}}$ approximately constant
Φ'_μ = sliding friction
Φ'_{creep} = the back calculated drained friction during creep with $c' = 0$
Φ'_g = geometrical interference friction, = Φ'_β and ≈ Φ″ as developed herein
$\Phi''_{residual}$ (or Φ'_{res}) = minimum Φ′ at very high shear strain
Φ″ = the part of Φ′ from the **D**-component, at a given structure in an **IDS**-test
Φ'_α = the part of Φ′ from the **I**-component (Eqn. 2), also referred to as "secondary shear"
Φ'_β = the part of Φ′ from the **D**-component ≈ Φ″, (Eqn. 3), also referred to as "primary shear"
$\Phi'_{\beta max}$ = the clay structure's current maximum Φ'_β capability
σ′ = normal stress, all stresses effective
σ'_c = isotropic consolidation stress
σ'_{cu} = unloaded σ'_c
$\overline{\sigma}_o$ = octahedral normal effective stress
σ'_1 = major principal stress
σ'_{1h} = high value in **IDS**-test (Fig 1c)
σ'_{1l} = lower value in **IDS**-test (Fig 1c)
σ'_3 = minor principal stress
σ'_t = normal stress on plane of **IDS**-test tangency (Fig. 1c)
$\overline{\sigma'}_1$ = $(\sigma'_{1h} + \sigma'_{1l})/2$
σ'_{vo} = vertical effective stress before a surcharge
$\Delta\sigma'_{vs}$ = vertical stress added by surcharge
τ = mobilized shear stress
τ_t = τ on plane of "t" (Fig. 1c)
τ_{AX}, τ_{BX} = mobilized shear at $Є_x$ in specimens A and B (Figs. 1a, 1b, and 1c)